Material Matters™

ALDRICH® *Chemistry*

Alternative Energy
Photovoltaics, Ionic Liquids, and MOFs
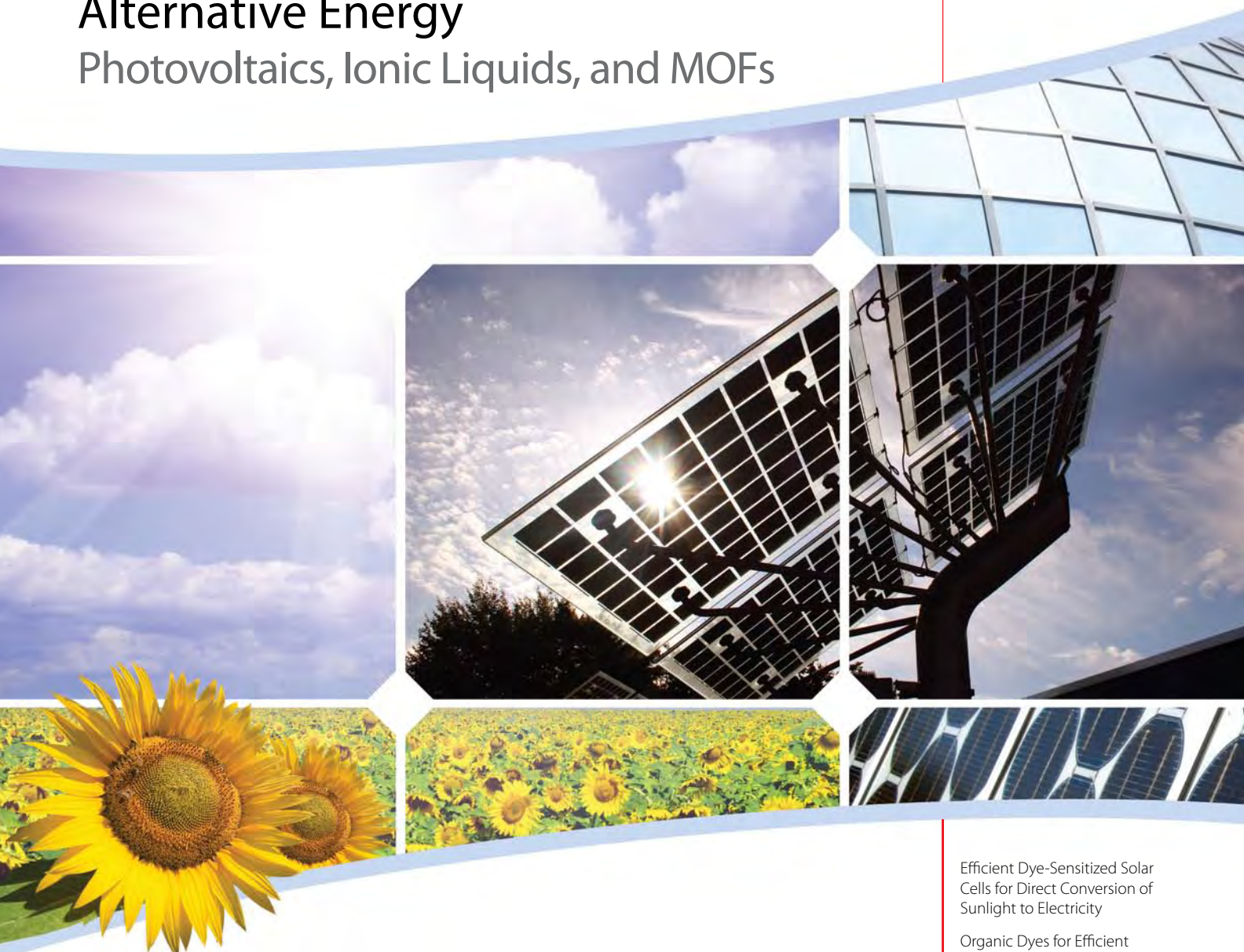
Solar energy—the energy for everyone

Efficient Dye-Sensitized Solar Cells for Direct Conversion of Sunlight to Electricity

Organic Dyes for Efficient and Stable Dye-Sensitized Solar Cells

The Relentless Rise of Disruptive Photovoltaics

Ionic Liquids for Energy Storage Applications

Selected Applications of Metal-Organic Frameworks in Sustainable Energy Technologies

SIGMA-ALDRICH®

Introduction

Over the coming decades, the demand for sustainable energy sources is expected to continuously grow in all areas of energy consumption including transportation, portable and consumer electronics, defense and special applications. To meet this new challenge, several alternatives to fossil fuels, the key energy sources of today, are being meticulously explored. One of the most attractive among them is solar energy, which can be converted into electricity by means of the photovoltaic effect, that is, the ability of certain semiconductors to generate an electric current when illuminated by sunlight.

A typical photovoltaic (PV) cell consists of two different types of semiconducting materials, one of which is doped with electron-rich additives (*n-type*) and another one with electron-poor (*p-type*) additives. When sunlight strikes the PV cell, a part of its energy is absorbed by electrons in the n-type material. The affected electrons leave their usual positions and become available for an electrical current. The voltage driving the electrical current in the device is generated by the *built-in electric field* that forms in the area of contact between n- and p-type components of the cell (the *p-n junction*). The circuit is completed by an external connection, which can be attached to a device consuming electrical energy (*load*).

Viktor Balema
Materials Science
Sigma-Aldrich Corporation

Photovoltaic cells can be classified into several generations indicating the order of their appearance on the market. First generation solar cells consist of large surface area, single junction devices, which are usually based on silicon technology. Their theoretical efficiency is relatively low and the energy payback period exceeds 5 years. The second generation materials had been developed to reduce production costs of solar cells without jeopardizing their energy output. They include cadmium telluride, copper indium gallium selenide, amorphous silicon or micromorphous silicon, which are applied as thin films on glass or ceramic substrates. The third generation of photovoltaic systems, known as multi-junction photovoltaic cells, aim to enhance the electrical performance of the second generation cells while maintaining very low production costs. They are produced using vapor deposition techniques and consist of multiple semiconductor layers capable of capturing different parts of the solar spectrum. Another type of thin film solar cells is represented by dye-sensitized systems (DSSC, DSC or DYSC), which consist of photo-sensitized semiconductors deposited on conducting oxide anodes and include a redox electrolyte. Finally, organic photovoltaic cells (OPVC), which use organic semiconductors for light absorption and charge transport, represent the fourth generation of solar energy converting devices.

Once converted into electricity, solar energy can power a variety of tools and devices. It can also be stored in chemical form in batteries, supercapacitors, in the form of hydrogen in metal organic frameworks, or carbon-based materials. Afterall, the solar energy chemically stored in coal, oil or natural gas is currently our major source of energy.

This issue of **Material Matters™** features five articles that are concerned with converting solar energy into electricity using the photovoltaic effect and storing it in chemical form for later use. The conversion of sunlight into electricity in highly efficient dye-sensitized solar cells is described in the article by K. Kalyanasundaram and M. Grätzel from Ecole Polytechnique Fédérale de Lausanne, Switzerland. Organic dyes for dye-sensitized solar cells are discussed in the paper by K. Hara and N. Koumura from the National Institute of Advanced Industrial Science and Technology (AIST), Japan. The status of photovoltaic research at the U.S. Department of Energy is highlighted in the contribution by S. Stephens. In a joint article by J.A. Irvin from Texas State University and J. Stenger-Smith from Naval Air Warfare Center, the researchers discuss ways of using ionic liquids in energy storage devices. Finally, metal-organic frameworks (MOFs) capable of storing significant amounts of hydrogen and other energy-rich gases are discussed in the article by S. Caskey, Sigma-Aldrich, and A. Matzger, University of Michigan, Ann Arbor.

The "Your Materials Matter" section of this issue features a material that has been brought to our attention by a leading researcher from the scientific community. Each article in this publication is accompanied by the corresponding Aldrich Materials Science products that are the key to fabricating devices in the field of Photovoltaics, Ionic Liquid based energy storage, and Metal-Organic Frameworks. The opposing page lists the material categories that you will find in this issue. For a comprehensive library of products and all associated information, please visit Aldrich Materials Science at *sigma-aldrich.com/matsci*. We welcome your comments and questions regarding **Material Matters™** or any materials of interest. Please contact us at matsci@sial.com.

About Our Cover

Reserves of solar energy are enormous. The amount of solar energy reaching the surface of our planet in one year is about twice as large as could ever be generated using all known reserves of coal, oil, natural gas, and mined uranium combined. Once improved to the limits of their theoretical capacity, photovoltaic cells, like the ones shown on the cover, will supply enough energy for all industrial and agricultural needs, space exploration, leisure, or any other activities of the human race (see the articles on pp. 88, 92, and 99). After all, the Earth receives more energy from the Sun per hour than our civilization consumes in a year.

"Your Materials Matter."

Joe Porwoll

Joe Porwoll, President
Aldrich Chemical Co., Inc.

Prof. Sesha S. Srinivasan of Tuskegee University kindly suggested that we offer Magnesium Borohydride (**Aldrich Prod. No. 715247**) as a material for alternative energy applications.[1] This complex metal hydride, produced by Aldrich Materials Science R&D, is a base-material for advanced energy storage systems with potential for fulfilling the United States Department of Energy's hydrogen storage goals.[2] Magnesium borohydride crystallizes in a hexagonal phase that is stable at room temperature. At 185 °C, the material converts to an orthorhombic phase, which persists and is stable upon cooling back to room temperature. Both phases consist of complex networks of corner-sharing tetrahedra including a central Mg atom and four BH_4 units.[3]
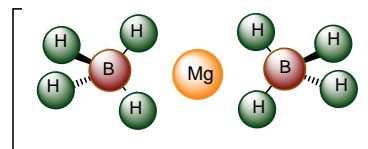
References:
(1) Jensen, C. M.; Severa, G.; Ronnebro, E.; Autrey, T.; Orimo, S. *Abstracts of Papers, 238th ACS National Meeting, Washington, DC, United States,* **2009**, FUEL-227.
(2) Read, C.; Thomas, G.; Ordaz, G.; Satyapal, S. *Material Matters* **2007**, *2.2,* 3.
(3) Soloveichik, G. *Material Matters* **2007**, *2.2,* 11

*Do you have a compound that you wish Sigma-Aldrich® could list to help materials research? If it is needed to accelerate your research, it matters—please send your suggestion to **matsci@sial.com** and we will be happy to give it careful consideration.*

Magnesium borohydride, 95%

[49855-95-0] $Mg(BH_4)_2$ FW 53.99

715247-1G	1 g

Alternative Energy Products Featured in this Issue

Materials Category	Content	Page
Metal Based Dyes for Dye-Sensitized Solar Cells	Organometallic dyes useful for fabricating dye-sensitized solar cells	90
Nanopowders for Photovoltaic Applications	Titanium and Zinc oxide based products for energy generation	91
Polyaromatic Dyes for Dye-Sensitized Solar Cells	Polyaromatic materials for use in photovoltaic applications	95
Photovoltaic Materials: Organic Semiconductors	A variety of n-type and p-type semiconductor materials	96
Photovoltaic Materials: ITO and Indium Oxide Powders	Indium Tin Oxide and Indium Oxides for energy applications	98
Thiophene Building Blocks for Photovoltaic Materials Design	Synthetic building blocks for creating new materials for photovoltaic applications	98
High Purity Metal Selenides and Tellurides	Metal selenides and tellurides for preparation of thin film photovoltaic materials	102
Ionic Liquids for Energy Applications	Low-melting ionic liquids for applications in energy generation and storage devices	106
Tetraalkyl Ammonium Salts for Electrochemistry	Tetraalkyl Ammonium Salts for electrolytes used in batteries, supercapacitors and other electrochemical systems	107
Electroactive Polymers	A selection of conducting polyacetylines, poly(phenylene sulfide)s, polyanilines, polypyrroles, and polythiophenes	107
Polythiophenes	Electroactive polymers for energy applications	109
Organic Linker Molecules for Metal-Organic Frameworks	Organic linker molecules for fabricating various types of 3D metal-organic frameworks	114
Selected Metal Salts for Synthesis of Metal-Organic Frameworks	A selection of metal salts used for the preparation of metal-organic frameworks	115
Selected Solvents for Synthesis of Metal-Organic Frameworks	Typical solvents for the preparation of metal-organic frameworks	115
Metal-Organic Frameworks (Basolite™)	The Sigma-Aldrich selection of metal-organic frameworks for Materials Science and Chemistry applications	115

For questions, product data, or new product suggestions, please contact Aldrich Materials Science at ***matsci@sial.com***.

87

Efficient Dye-Sensitized Solar Cells for Direct Conversion of Sunlight to Electricity

Kuppuswamy Kalyanasundaram* and Michael Grätzel
Laboratory for Photonics and Interfaces (LPI), Ecole Polytechnique
Fédérale de Lausanne (EPFL), CH-1015 Lausanne, Switzerland
*Email: k.kalyanasundaram@epfl.ch

Introduction

Sunlight is an abundant natural resource and for many decades scientists have been interested to find ways and means of harnessing the energy from the sun. Researchers have explored many processes where solar irradiation can be used to create an ecologically healthy environment. Examples range from energy storage to degradation of atomic waste. A very attractive direct route for solar energy conversion and storage, with a high potential impact is the production of electricity. With electrical power stored in batteries, it is possible to do a wide variety of things on the go. Advances in the synthesis of materials and experimental tools that permit manipulation or engineering at the molecular level have given impetus to the design of photonic and opto-electronic devices from a bottom-up type approach. One such device that our laboratory has been developing and optimizing for many years is a thin film solar cell that is based on dye-sensitization of wide bandgap semiconductors, in the form of nanocrystalline films. **Figure 1** shows a schematic design of the dye-sensitized solar cell (DSC).
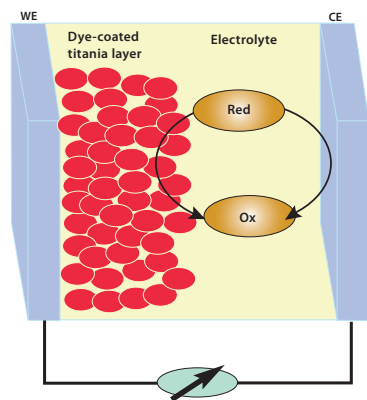
Figure 1. Schematic representation of a dye-sensitized thin layer solar cell.

An exploded view of its components and assembly structure is shown in **Figure 2**. A dye-sensitized solar cell (DSC), in essence, is a sandwich structure made of two conducting oxide electrodes with an organic redox electrolyte filling the interlayer separation. The heart of the solar cell is the mesoporous wide bangap oxide layer deposited onto a conducting oxide substrate. This oxide layer is composed of nano-sized particles that have been sintered together to allow electronic conduction to take place. It has a spongy-like structure that upon immersion in a dye solution picks up the dye molecules giving an intense coloration. Exposure of the solar cell to visible light leads to electronic excitation of the dye, D, to an excited state form (D*), which can inject electrons to the conduction band of the oxide

semiconductor. The original state of the dye D (D$^+$) is subsequently restored by the reduction of the oxidized form of the dye by the redox electrolyte. In the most extensively studied version of DSC, the electrolyte is an iodide/triiodide mixture dissolved in an organic medium.
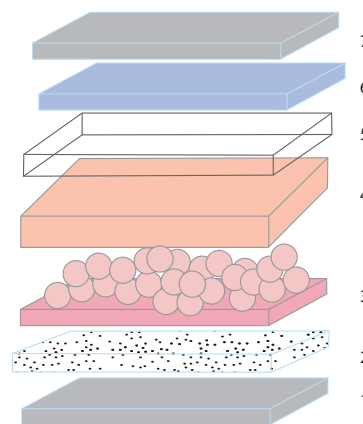
Figure 2. Exploded view of a dye-sensitized solar cell showing key components: 1) transparent conducting oxide, TCO (working electrode, WE); 2) underlayer (mesoporous oxide); 3) photoactive mesoporous oxide with coated dye molecules; 4) electrolyte containing redox mediators; 5) sealing gasket/separator; 6) finely divided Pt catalyst layer and 7) transparent conducting oxide, TCO (counter-electrode, CE).

Electrons injected in the oxide layer hop through the network of the nano-sized particles to reach the back collector electrode. Under closed circuit conditions, the electrons flow over the external circuit to arrive at the counter electrode and reduce the oxidized form of the redox mediator. This sequence of reactions constitute a light-induced oxidation-reduction cycle or photosensitization of the semiconductor electrode. In the most extensively studied version, a polypyridine complex of Ru such as {Ru(4,4'-(COOH)$_2$bpy)$_2$(SCN)$_2$} (N3, **Aldrich Prod. No. 703206**) is used as the dye, together with an iodide/triiodide redox couple in methoxypropionitrile (**Aldrich Prod. No. 65290**) solvent, which is used as the redox electrolyte. A variant of this system uses a hole transport material, a triarylamine deriviate, 2,2',7,7'-tetrakis-(N,N-di-p-methoxyphenylamine)-9,9'-spirobithuorene, (spiro-OMeTAD), as an electron mediator instead of the (iodide-triiodide) mixture. The advantage of the spiro-OMeTAD based DSC version is that it is a solvent-free, quasi-solid state system that can be packaged for portable electronics.

Advantages of the Mesoporous Oxide Layers

Photosensitzation of semiconductors had been examined earlier[1-8] with single crystal electrodes and the process was found to be relatively inefficient. Observed photocurrents were very low (few µA/cm^2), leading to an overall light conversion efficiency of <<1%. Several unique features of the DSC allow pronounced enhancement of the light energy efficiency. Using mesoporous structures, it is possible to control the dye distribution on the surface to achieve locally high concentrations without any side effects. The available surface area for dye distribution is considerably high in a mesoporous structure (surface roughness factor >1,000) and as such it is possible to achieve monolayer coverage without concentration quenching as observed on flat surfaces.[1-8] It is also possible to have absorbance of >3 permitting near total absorption of visible light. However, increasing the surface area can lead to lower efficiencies due to the promotion of charge recombination before

charges arrive at the collector electrode. Excited state charge injection of an anchored dye to the conduction band of the oxide semiconductor permits a design where the forward electron transfer can occur much faster compared to the backward electron movement, i.e., relaxation of the dye to its ground state. A five to six orders of magnitude difference is feasible permitting near quantitative scavenging of all injected electrons. In homogeneous solvents, back electron transfer tends to occur very rapidly, often within the primary cage itself. In addition to the above differences due to the morphology of the dye-coated oxide substrate, there are other important effects that are responsible for the high overall efficiency of this type of solar cell. In contrast to the flat surfaces of macro-electrodes, a high concentration (typically 0.5 M) of iodide ions in the electrolyte effectively screens out any macroscopic electric fields. Charge separation is primarily driven by the inherent energetics (redox potentials) of the different species at the TiO_2/dye/electrolyte interface rather than by the presence of macroscopic, electrostatic, potential energy gradients.

Progress and Challenges

The DSC research field can be an exciting playground for synthetic and materials scientists. Unlike single material-based crystalline semicon-ductor solar cells, DSCs have several key components which allow numerous innovative approaches. DSCs are being developed in many different textures and compositions, and display a variety of properties. In the following sections, we highlight some of the novel advancements being tested with a wide variety of chemical components. It has been possible to design DSC panels where the oxide layer is optically translucent to opaque; flexible, lightweight versions based on polymer supports in lieu of glass substrates (ideal for portable electronics) and also versions created in a variety of colors. Examination of numerous dyes of different chemical structure and functional groups has permitted identification of the key requirements for efficient sensitization:

• Significant light absorption in the visible-near IR region to allow maximum harvesting of solar photons
• Low-lying excited states formed in high quantum yield capable of participating in electron transfer processes
• Position of the energy levels of the dye in the ground and excited states to permit efficient injection of charges from the excited states into the semiconductor conduction bound while also permitting quantitative regeneration of the dye by the redox mediators
• Presence of suitable anchoring groups that promote efficient coupling of the dye excited state with the acceptor levels of the semicon-ducting oxide
• Adequate chemical stability of the dye in its oxidized form to permit extensive redox cycling

Many different dyes with a variety of chromophoric ligands have been synthesized and studied in DSCs: polypyridine complexes of transition metals, metalloporphyrins, and metallo-phathalocyanines as well as different metal-free, donor-acceptor type dyes. **Figure 3** illustrates the tunability of colors in the design of DSCs.

Figure 3. Tuning of colors of dye-sensitized solar cell. Printed with permission from Schott AG.

Polypyridine complexes of Ru have been the first choice of dyes in most of the studies due to the vast knowledge accumulated over the years in regards to their photophysics and photoredox chemistry. Synthetically, it is easy to vary the level of conjugation of the polypyridine ligand systems and introduce suitable groups in the periphery of the ligands to induce and tune both spectral and redox properties. Coordination compounds of the general structure ML2X2, where L stands for 2, 2'-dicarboxybipyridine (dcbpy), M= Ru(II) or Os(II) and X represents a halide, cyanide, thiocyanate, acetyl acetonate, or thiocarbamate, and have been found to be efficient sensitizers. Ru-complexes based on carboxy bpy or carboxy terpy such as N3 (**Aldrich Prod. No.** 703206), N719 (**Aldrich Prod. No.** 703214), Z907 (**Aldrich Prod. No.** 703168) and "black dye" (tris(cyanato)-2,2'-2"-terpyridyl-4,4',4"-tricarboxylate)Ru(II) are used worldwide as benchmark reference dyes. **Figure 4** shows the structures of some of these high performance dyes:
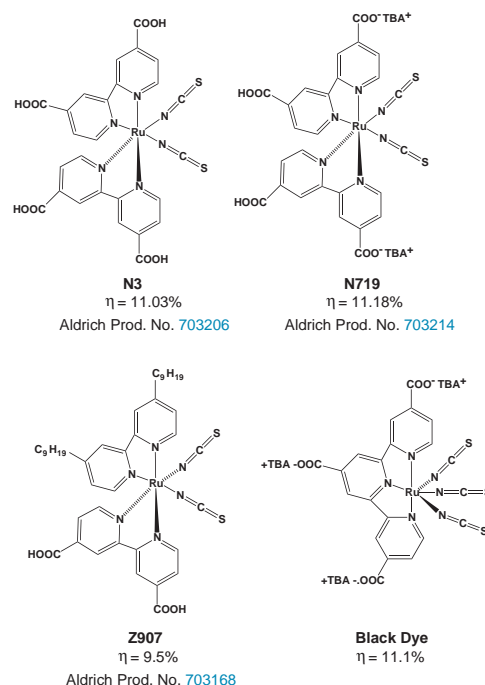
Figure 4. Structures of some of the most efficient Ru-dyes for dye solar cells.

For coumarin or polyene-type organic dyes, strikingly high solar conversion efficiency reaching up to 9.2% has been reported by Arakawa, Uchida and coworkers.[1-3] Molecular engineering of the interface is important to obtain high efficiencies. Additives that promote desegregation of the dye molecules and alkylamine donors help control the surface properties of the oxide. In addition to reducing the dark currents, they allow a higher fill factor.

State of the Art Performance

Solar cell research and development takes place at three levels. Primary optimization studies are done usually in small (<1 cm^2 area) cells. Modules are the second phase of solar cell development and are larger in size (typically 25-100 cm^2). The third stage involves large area terrestrial units for solar power generation which are much larger and composed of many modules connected in series or parallel. Typical panel sizes are 0.5 to 2 m^2. Extensive research in many laboratories across the globe has led to significant progress in obtaining increasingly higher solar light conversion efficiencies, both at the lab cell levels and also in larger modules.

For questions, product data, or new product suggestions, please contact Aldrich Materials Science at *matsci@sial.com*.

89

Tables 1 and **2** provide a summary of the best performance data obtained (state of the art) to date in solar light conversion, as well as open circuit voltages (V$_{OC}$) at various fill factors (FF) using various dyes for a number of surface areas.

Table 1. Record efficiencies of DSC of various device sizes.

Dye	Surface (cm²)	η (%)	V$_{OC}$ (V)	I$_{SC}$ (mA*cm^{-2})	FF (%)
N-719	<1	11.2	0.84	17.73	74
N-749	0.219	11.1	0.736	20.9	72
N-749	1.004	10.4	0.72	21.8	65
N-719	1.31	10.1	0.82	17	72
N-3	2.36	8.2	0.726	15.8	71
N-749	26.5 (sm)	6.3	6.145	1.7	60

N-719, N-749, and N-3 are codes for molecular structures as seen in **Figure 4**. All systems employ a liquid electrolyte mixture of (iodide/triiodide) in a low-viscosity solvent. Previously unpublished data.

Improvement in the light absorption properties of the dyes particularly in the near-IR region (700-900 nm) will lead to higher photocurrents and light conversion efficiency.

Table 2. Efficiency of DSC lab-cells, sub-modules and modules obtained in recent years in different industrial laboratories in Japan. Previously unpublished data.

Lab.	Surface (cm²)	η (%)	V$_{OC}$ (V)	I$_{SC}$ (mA*cm^{-2})	FF (%)	Date
Dai Nippon	0.16	6.52	0.746	12.88	0.678	2007
Fujikura	25	7.33	0.778	13.788	0.683	2008
NGK	0.25	7.66	0.701	16.4	0.668	2008
NGK	60.86 (8×8)	7.04	0.735	16	0.628	2008
ENOES	72.2 (10×10)	6.3	0.78	12.5	0.65	2005
ENOES	72.2	7.25	0.78	13.94	0.67	2007
PECCELL	0.23	5.9	0.705	14.1	0.59	2008
Sharp	1.004	10.4	0.729	21.8	0.65	2005
Sharp	25.45	9.2		19	0.61	2007
Sony	18.5	8.2	0.659	19.8	0.629	2008

For practical applications, dye solar cells have to meet stringent stability requirements. For a lifespan of >10 years, the dyes have to be stable to reversibly undergo millions of oxidation and reduction cycles. In tropical countries, surface panel temperatures can easily exceed 60 °C. Hence, solar cell modules should be tested for stability at elevated temperatures up to 80 °C under high humidity conditions. With low boiling solvents, corrosion of the seal can also create stability problems. For this reason, current efforts are directed towards using low-temperature molten salts (ionic liquids) such as alkylimiadazolium halides. Using long-chain alkyl substituents on the bpy ligand as in the dye Z907 and ionic liquid based electrolytes, it is possible to maintain redox stability for over 1,000 hours of continuous illumination. Outdoor studies of modules have demonstrated several unique features of DSCs, such as higher solar energy conversion under diffuse light conditions and positive temperature coefficients. References listed below provide more detailed information about recent advances in the field of dye-sensitized solar cells.

References:
(1) Horiuchi, T.; Miura, H.; Sumioka, K.; Uchida, S. *J. Am. Chem. Soc.* **2004**, *126*, 12218.
(2) Hara, K.; Sato, T.; Katoh, R.; Furube, A.; Yoshihara, T.; Murai, M. *Adv. Functional Mat.* **2005**, *15*, 246.
(3) Ito, S.; Zakeeruddin, S. M.; Humphry-Baker, R.; Liska, P.; Charvet, R.; Cornte, P. *Adv. Materials* **2006**, *18*, 1202.
(4) Zakeeruddin, S. M.; Grätzel, M. *Adv. Functional Mater.* **2009**, *19*, 1.
(5) Mishra, A.; Fischer, M. K. R.; Bauerle, P. *Angew Chem.* **2009**, *48*, 6674.
(6) Nazeeruddin, Md. K.; Grätzel, M. *Struc & Bonding* **2007**, *123*, 113.
(7) Hagfeldt, A.; Grätzel, M. *Chem Rev.* **1995**, *95*, 49.
(8) Kalyanasundaram, K.; Grätzel, M. *Coord. Chem. Rev.* **1998**, *177*, 347.
(9) Hodes, G. *J. Phys. Chem. C.* **2008**, *112*, 17778.
(10) Peter, L. M. *Phys. Chem. Chem. Phys.* **2007**, *9*, 2630.
(11) Peter, L. M. *J. Phys. Chem. C.* **2007**, *111*, 6601.
(12) Bisquert, J. *Phys. Chem. Chem. Phys.* **2008**, *10*, 49.
(13) Yum, J.-H.; Chen, P.; Grätzel, M.; Nazeeruddin, Md. K. *ChemSusChem* **2008**, *1*, 699.
(14) Gorlov, M.; Kloo, L. *Dalton Trans.* **2008**, 2655.

Metal Based Dyes for Dye-Sensitized Solar Cells

For a complete list of OPV dye materials, please visit *sigma-aldrich.com/opvdyes*

Name	Structure	Purity	Spectroscopic Properties	Cat. No.
Di-tetrabutylammonium *cis*-bis (isothiocyanato)bis(2,2'-bipyridyl-4,4'-dicarboxylato)ruthenium(II), (N-719) *		95%	λ$_{max}$ = 313, 393, 534 nm	703214-250MG
cis-Bis(isothiocyanato)(2,2'-bipyridyl-4,4'-dicarboxylato)(4,4'-di-nonyl-2'-bipyridyl)ruthenium(II), (Z-907) *		95%	λ$_{max}$ = 531, 295, 314 nm	703168-250MG
cis-Bis(isothiocyanato)bis(2,2'-bipyridyl-4,4'-dicarboxylato)ruthenium(II), (N-3) *		95%	λ$_{max}$ = 534, 312, 395 nm	703206-250MG

* Product of Dyesol, Ltd.

Name	Structure	Purity	Spectroscopic Properties	Cat. No.
Tris[2-(benzo[*b*]thiophen-2-yl) pyridinato-C^3,*N*]iridium(III)		96%	λ_{max} = 324 nm, λ_{em} = 595 nm in chloroform	680877-250MG
Tris[2-(4,6-difluorophenyl)pyridi-nato-C^2,*N*]iridium(III)		96%	λ_{max} = 347 nm, λ_{em} = 480 nm in chloroform	682594-250MG
Tris[2-phenylpyridinato-C^2,*N*]iridi-um(III)		96%	λ_{max} = 282 nm, λ_{em} = 507 nm in chloroform	694924-250MG
Tris[1-phenylisoquinoline-C^2,*N*] iridium(III)		-	λ_{max} = 324 nm, λ_{em} = 615 nm in tetrahydrofuran	688118-250MG
Tris(dibenzoylmethane) mono (1,10-phenanthroline)europium (III)		95%	λ_{max} = 228 nm, λ_{em} = 615 nm in tetrahydrofuran	538965-250MG
Copper(II) phthalocyanine		-	λ_{max} = 678 nm, λ_{em} = 404 nm	546674-1G
Copper(II) phthalocyanine		>99.99% trace metals basis	λ_{max} = 678 nm, λ_{em} = 404 nm	702854-500MG
Tris-(8-hydroxyquinoline)alumi-num		99.995% trace metals basis	λ_{max} = 259 nm, λ_{em} = 519 nm	697737-1G

Nanopowders for Photovoltaic Applications

For a complete list of materials for energy generation and storage, please visit *sigma-aldrich.com/renewable*

Name	Purity	Dimensions	Concentration (wt. %)	Cat. No.
Aluminum oxide	≥99.8%	avg. part. size 13 nm, surface area 85-115 m²/g	-	718475-100G
Titanium dioxide	≥99.5%	avg. part. size 21 nm, spec. surface area 35-65 m²/g (BET)	-	718467-100G
Titanium(IV) oxide, anatase	99.7% trace metals basis	particle size <25 nm, spec. surface area 200-220 m²/g	-	637254-50G 637254-100G 637254-500G
Titanium(IV) oxide, mixture of rutile and anatase	99.5% trace metals basis	particle size <50 nm (XRD) particle size <100 nm (BET)	-	634662-25G 634662-100G
Titanium(IV) oxide, mixture of rutile and anatase	99.9% trace metals basis	particle size <250 nm (DLS) particle size ~21 nm primary particle size of starting nanopowder, BET surf. area 50 m²/g (BET surface area of starting nanopowder)	53-57 in diethylene glycol monobutyl ether/ ethylene glycol	700355-25G
Titanium(IV) oxide, mixture of rutile and anatase	99.9% trace metals basis	particle size <150 nm (DLS) particle size ~21 nm primary particle size of starting nanopowder	33-37 in H₂O	700347-25G 700347-100G
Titanium(IV) oxide, rutile	99.5% trace metals basis	particle size <100 nm, spec. surface area 130-190 m²/g	-	637262-25G 637262-100G 637262-500G
Zinc oxide	-	particle size <100 nm, surface area 15-25 m²/g	-	544906-10G 544906-50G
Zinc oxide	>97%	particle size <50 nm (BET), >10.8 m²/g	-	677450-5G

For questions, product data, or new product suggestions, please contact Aldrich Materials Science at *matsci@sial.com*.

Organic Dyes for Efficient and Stable Dye-Sensitized Solar Cells
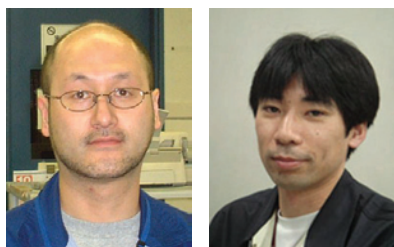
Kohjiro Hara[1] and Nagatoshi Koumura[2]

National Institute of Advanced Industrial Science and Technology (AIST),
[1]Research Center for Photovoltaics and [2]Photonics Research Institute
1-1-1 Higashi, Tsukuba, Ibaraki 305-8565, Japan
Email: k-hara@aist.go.jp, n-koumura@aist.go.jp

Introduction

Over the last decade, dye-sensitized solar cells (DSSCs) have attracted much attention because these unconventional solar cells exhibit high performance and have the potential for low-cost production.[1-4] Recently, solar energy-to-electricity conversion efficiencies as high as 11% under AM 1.5 G irradiation have been attained with DSSCs.[5-7] In DSSCs, the photosensitizer is one of the most important components influencing solar cell performance, because the choice of sensitizer determines the photoresponse of the DSSC and initiates the primary steps of photon absorption and the subsequent electron transfer process. Generally, Ru-polypyridyl-complex sensitizers, e.g., *cis*-dithio-cyanato bis(4,4'-dicarboxy-2,2'-bipyridine)ruthenium(II) (called N3 (**Aldrich Prod. No.** 703206) or N719 (**Aldrich Prod. No.** 703214) dyes) developed by Prof. Grätzel and coworkers, have been employed for efficient DSSCs.[4,5]

In addition to conventional Ru-complex sensitizers, metal-free analogs in the form of organic dyes have also been investigated in DSSCs. The photovoltaic performance of organic-dye sensitizers has continually improved.[8-14] Organic dyes have several advantages as sensitizers: (a) there are fewer concerns about limited resources, because they do not contain noble metals such as ruthenium, (b) they have large absorption coefficients due to intramolecular π-π* transitions, and (c) there are a wide variety of structures, each of which are relatively easy to modify.

However, the performance of DSSCs based on organic dyes has not yet exceeded those based on Ru complexes. To achieve higher performances for solar cells based on organic dyes, comparable to those for solar cells based on Ru complexes, sophisticated molecular design of organic dyes is required. For this purpose, we have designed and synthesized alkyl-functionalized carbazole dyes (**MK** dyes) in an effort to improve both solar cell performance and long-term stability of the solar cells.[15-17] Here, we report the detailed molecular design of **MK** dyes and the photovoltaic performance and long-term stability of DSSCs based on them.

Structure and Operating Principle of DSSC

Figure 1 shows a schematic of a DSSC and presents the mechanism of electric power generation in the DSSC. First, a sensitizer molecule, which is adsorbed on the surface of a nanocrystalline TiO_2 electrode, absorbs the incident photon flux and is excited from the ground state (S) to the excited state (S*). One type of photoexcitation causes transfer of an electron from the highest occupied molecular orbital (HOMO) of the sensitizer to its lowest unoccupied molecular orbital (LUMO). Subsequent injection of the excited electron into the conduction band of the TiO_2 electrode results in oxidation of the sensitizer molecule. The injected electron diffuses through the TiO_2 electrode toward the transparent conducting oxide (TCO)-coated electrode and through the external load and wiring, eventually reaches the counter electrode. The oxidized sensitizer is reduced by I^- ions in the electrolyte, regenerating the ground state of the sensitizer, and I^- ions are oxidized to I_3^- ions. The I_3^- ions diffuse toward the counter electrode where they are reduced back to I^- ions. Overall, electric power is generated without permanent chemical transformation.
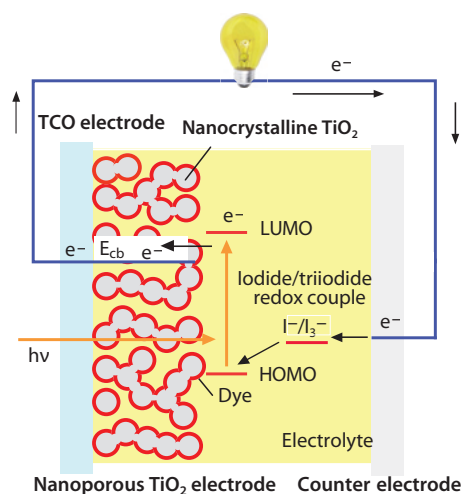
Figure 1. Schematic of a DSSC illustrating the mechanism of electric power generation.

The photocurrent produced in a DSSC is directly influenced by the properties of the sensitizer. For example, the energy gap between the HOMO and LUMO of the sensitizer (which corresponds to the band gap, E_g, for inorganic semiconductor materials) determines the photoresponse range of the DSSC. Absorption over a wide range of wavelengths, extending into the near-IR region due to a small HOMO-LUMO energy gap, is necessary for harvesting a large fraction of the solar spectrum, which in turn produces a large photocurrent and thus highly efficient solar cell performance. In addition, the energy levels of the HOMO and LUMO must match the iodine redox potential and the E_{cb} of the TiO_2 electrode. For electron injection, the LUMO must be sufficiently more negative (higher energy) than the TiO_2 E_{cb}; the energy gap between the two levels is the driving force for electron injection. The HOMO must be sufficiently more positive (lower energy) than the redox potential of I^-/I_3^- to accept electrons effectively. Thus, the molecular structure of the sensitizer must be strategically designed so that its properties are optimal for efficient DSSC performance.

Molecular Structure of MK Dyes

Molecular structures of two of the **MK** dyes (**MK-2** and **MK-14**) are shown in **Figure 2**. These molecules consist of a donor moiety (carbazole unit) and an acceptor moiety (cyanoacrylic acid) connected by a π-conjugated structure of an oligothiophene moiety. This donor-acceptor structure gives a strong absorption with a large absorption coefficient in the visible region due to the intramolecular π-π* transition. The absorption peak (λ_{max}) is observed at 480 nm[16] for **MK-2** and 483 nm[17] for **MK-14** in tetrahydrofuran-toluene (20:80 vol %) solution. The molar absorption coefficient ε at λ_{max} for **MK-2** and **MK-14** is 38,400[16] and 36,200 M^{-1} cm^{-1},[17] respectively. In addition, these organic dyes have a carboxy group as an anchoring group to adsorb onto the nanocrystalline TiO_2 electrode.
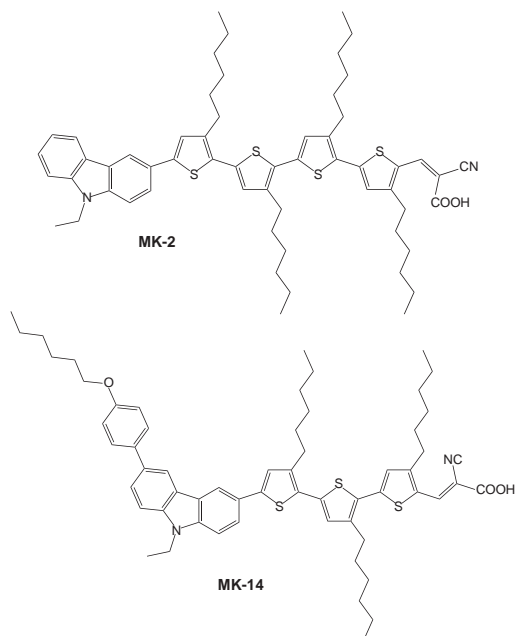
Figure 2. Molecular structures of alkyl-functionalized carbazole (MK) dyes.

Furthermore, an important feature of this new organic dye is the presence of *n*-hexyl substituents on the oligothiophene backbone. We expected that the long alkyl chains would decrease strong π-π* stacking interaction between molecules, decreasing electron injection yield, and physically restrain the I_3^- ions away from the TiO_2 surface and consequently decrease charge recombination between the electrons and I_3^- ions. Thus, new strategic molecular designs of organic dyes in terms of engineering the interface between the organic dyes and the TiO_2 surface are required to improve photovoltaic performance of organic DSSCs.

Solar Cell Performance of the DSSCs Based on MK Dyes

The spectrum of incident photon-to-current conversion efficiency (IPCE) for a DSSC composed of a nanocrystalline TiO_2 electrode, **MK-2**, and an iodine redox (I^-/I_3^-) electrolyte is shown in **Figure 3**.
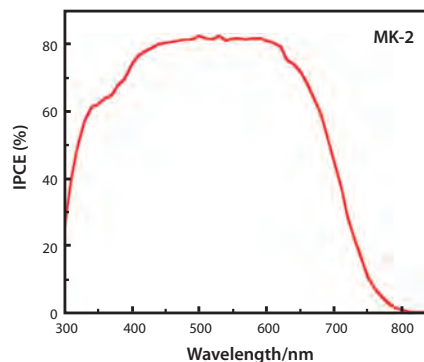
Figure 3. The incident photon-to-current conversion efficiency (IPCE) spectrum for a DSSC based on MK-2.

Photons with a wide range of wavelengths (350-800 nm) can be converted to current by DSSCs based on this dye. IPCE values higher than 70% were observed at 400-650 nm; the maximum being 80% at 498 nm. When the reducing effect of reflection and absorption losses in the TCO substrate are excluded, the photon-to-current conversion efficiency in this range exceeds 90%, which indicates highly efficient performance of these solar cells. The solar energy-to-electricity conversion efficiency, η (%), of solar cells can be estimated from the following equation:

$$\eta(\%) = \frac{J_{sc} \times V_{oc} \times FF}{I_0} \times 100$$

where I_0 is the photon flux (ca. 100 mW cm^{-2} for AM 1.5 G), J_{SC} is the short-circuit current density under irradiation, V_{OC} is the open-circuit voltage, and *FF* is the fill factor. After optimization of the solar cell, we attained high η values of 8.3%[16] (J_{SC} = 15.2 mA cm^{-2}, V_{OC} = 0.73 V, and *FF* = 0.75, as shown in **Figure 4**) and 8.1%[17] (J_{SC} = 16.0 mA cm^{-2}, V_{OC} = 0.71 V, and *FF* = 0.71) with DSSCs based on **MK-2** and **MK-14**, respectively, under simulated AM 1.5 G irradiation (100 mW cm^{-2} with an aperture mask and without an anti-reflection film); the electrolyte was 0.6 M 1,2-dimethyl-3-*n*-propylimidazolium iodide (**Aldrich Prod. No. 49637**)-0.1M LiI (**Aldrich Prod. No. 450952**)-0.2M I_2 (**Aldrich Prod. No. 451045**)-0.5M 4-*tert*-butylpyridine (**Aldrich Prod. No. 142379**) in acetonitrile.
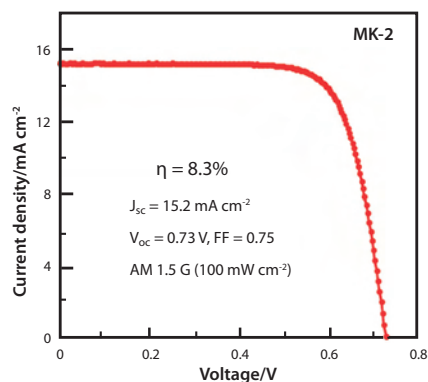
Figure 4. The photocurrent density versus voltage curve for a DSSC based on MK-2.

In addition, a DSSC based on **MK-2** and an ionic liquid (IL)-based electrolyte showed an η value of 7.6% (J_{SC} = 13.9 mA cm^{-2}, V_{OC} = 0.73 V, and *FF* = 0.75), which was comparable to that with a volatile liquid electrolyte.[18]

For questions, product data, or new product suggestions, please contact Aldrich Materials Science at *matsci@sial.com*.

93

Electron Diffusion Length

In DSSCs, electron transport in nanocrystalline TiO$_2$ electrodes is also important for high solar cell performance because this process competes with charge recombination between electrons and dye cations and between electrons and redox ions (I$_3^-$), which represent the loss processes in the system. For the photogenerated electrons to be collected, electron transport in the nanocrystalline TiO$_2$ electrode must predominate over both charge-recombination processes. The electron-transport kinetics in nanocrystalline TiO$_2$ electrodes are defined by the electron diffusion length (L) as shown in the following equation:

$$L = \sqrt{D \cdot \tau}$$

where D is the electron diffusion coefficient, and τ is the electron lifetime. For example, the τ values for DSSCs with conventional coumarin dyes were much shorter than the value for DSSCs based on a Ru complex, which suggests that charge recombination between conduction-band electrons in the TiO$_2$ and I$_3^-$ ions in the electrolyte occurs more easily in solar cells based on coumarin dyes. From this result, we concluded that the shorter τ values, which result in shorter L values, for DSSCs based on organic dyes relative to those based on Ru complexes lead to lower performance of DSSCs with organic dyes than those for DSSCs with Ru complexes.

As mentioned, an important feature of **MK** dyes is the presence of *n*-hexyl substituents on the oligothiophene backbone. We found that the τ values for the DSSCs based on **MK** dyes, which bear alkyl chains, were longer than the values for the DSSCs based on other organic dyes, which have thiophenes without alkyl chains.[15-18] We concluded that the long alkyl chains prevent the approach of I$_3^-$ ions to the TiO$_2$ surface due to a steric effect, a hydrophobic effect, or both, thereby decreasing the concentration of I$_3^-$ ions near the TiO$_2$ surface, and thus reducing charge recombination between the electrons and I$_3^-$ ions and increasing the τ value. Our success with these alkyl-functionalized **MK** dyes strongly suggests that the photovoltaic performance of DSSCs based on organic-dye sensitizers can be improved further.

Long-Term Stability of Solar Cell Performance

Figure 5 shows long-term stability data for a DSSC based on **MK-2** and an IL-based electrolyte (0.1M LiI-0.4M I$_2$-0.1M TBP in 1-methyl-3-*n*-propylimidazolium iodide, **Aldrich Prod. No.** 49637) under continuous AM 1.5 G irradiation through a UV (<420 nm) cut-off filter at ca. 50 °C. No decrease in the η was observed over a period of more than 2,000 hours (**Figure 5**).[19] This result clearly indicated that the DSSC based on **MK-2** was stable under visible-light irradiation at a relatively low temperature.
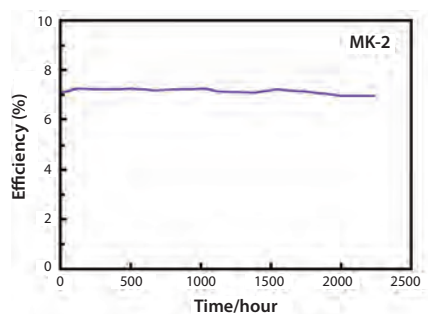
Figure 5. Long-term stability of a DSSC based on MK-2 with an ionic liquid electrolyte under visible-light irradiation.

We reported stability of organic dyes adsorbed on nanocrystalline TiO$_2$ electrodes under visible light irradiation.[20, 21] We observed good stability of **MK-2**, which has an oligothiophene moiety, under visible light irradiation, while dyes without the oligothiophene moiety showed significantly faster decomposition. The data of transient absorption spectroscopy measurement suggested that delocalization of holes on the oligothiophene moiety of **MK-2** leads to high stability of the dye cation after photoexcitation.[20] This result also indicates that **MK-2** and its cation are relatively stable under visible light irradiation due to its oligothiophene moiety. The performance of the DSSC decreased gradually under white-light irradiation including UV light or at 80 °C under dark conditions with no decomposition or detachment of the dye molecule from the TiO$_2$ electrode.[21] These results indicate that the **MK-2** dye molecule in the cell was stable even under white-light irradiation and at 80 °C under dark conditions. We conclude that there are other factors decreasing the solar cell performance after white-light irradiation and heating at 80 °C, and as such, the detailed mechanism is currently under further investigation.

Summary

We designed and synthesized alkyl-functionalized carbazole dyes (**MK** dyes) for use in DSSCs. The DSSCs based on **MK** dyes showed both high solar cell performance of up to 8% under simulated AM 1.5 G irradiation and good long-term stability under continuous simulated solar light (visible-light irradiation). One of most important features of **MK** dyes is the presence of a *n*-hexyloligothiophene backbone, which prevents charge recombination between electrons and I$_3^-$ ions on the TiO$_2$ electrode, and improves the stability of the dye molecule and the solar cell performance. Our results strongly suggest that the **MK** dyes can be successfully designed for use in DSSCs and further demonstrate the promising performance of DSSCs based on organic dye sensitizers.

References:
(1) O'Regan, B.; Grätzel, M. *Nature* **1991**, *353*, 737.
(2) Smestad, G.; Bignozzi, C.; Argazzi, R. *Sol. Energy Mater. Sol. Cells* **1994**, *32*, 259.
(3) Kay, A.; Grätzel, M. *Sol. Energy. Mater. Sol. Cells* **1996**, *44*, 99.
(4) Hagfeldt, A.; Grätzel, M. *Acc. Chem. Res.* **2000**, *33*, 269.
(5) Nazeeruddin, M. K.; De Angelis, F.; Fantacci, S.; Selloni, A.; Viscardi, G.; Liska, P.; Ito, S.; Takeru B.; Grätzel, M. *J. Am. Chem. Soc.* **2005**, *127*, 16835.
(6) Chiba, Y.; Islam, A.; Watanabe, Y.; Komiya, R.; Koide, N.; Han, L. *Jpn. J. Appl. Phys.* **2006**, *45*, L638.
(7) Cao, Y.; Bai, Y.; Yu, Q.; Cheng, Y.; Liu, S.; Shi, D.; Gao, F.; Wang, P. *J. Phys. Chem. C.* **2009**, *113*, 6290.
(8) Horiuchi, T.; Miura, H.; Sumioka, K.; Uchida, S. *J. Am. Chem. Soc.* **2004**, *126*, 12218.
(9) Hara, K.; Wang, Z.-S.; Sato, T.; Furube, A.; Katoh, R.; Sugihara, H.; Dan-oh, Y.; Kasada, C.; Shinpo A. Suga, S.; *J. Phys. Chem. B* **2005**, *109*, 15476.
(10) Qin, P.; Yang, X.; Chen, R.; Sun, L.; Marinado, T.; Edvinsson, T.; Boschloo, G.; Hagfeldt, A. *J. Phys. Chem. C* **2007**, *111*, 1853.
(11) Ito, S.; Miura, H.; Uchida, S.; Takata, M.; Sumioka, K.; Liska, P.; Comte, P.; Péchy, P.; Grätzel, M. *Chem. Commun.* **2008**, 5194.
(12) Wang, Z.-S.; Cui, Y.; Dan-Oh, Y.; Kasada, C.; Shinpo, A.; Hara, K. *J. Phys. Chem. C.* **2007**, *111*, 7224.
(13) Choi, H.; Baik, C.; Kang, S. O.; Ko, J.; Kang, M.-S.; Nazeeruddin, Md. K.; Grätzel, M. *Angew. Chem. Int. Ed.* **2008**, *47*, 327.
(14) Zhang, G.; Bala, H.; Cheng, Y.; Shi, D.; Lv, X.; Yu, Q.; Wang, P. *Chem. Commun.* **2009**, 2198.
(15) Koumura, N.; Wang, Z-S.; Mori, S.; Miyashita, M.; Suzuki, E.; Hara, K. *J. Am. Chem. Soc.* **2006**, *128*, 14256 (Addition and correction, **2008**, *130*, 4202).
(16) Wang, Z-S.; Koumura, N.; Cui, Y.; Takahashi, M.; Sekiguchi, H.; Mori, A.; Kubo, T.; Furube, A.; Hara, K. *Chem. Mater.* **2008**, *20*, 3993.
(17) Koumura, N.; Wang, Z-S.; Miyashita, M.; Sekiguchi, H.; Cui, Y.; Mori, A.; Mori, S.; Hara, K. *J. Mater. Chem.* **2009**, *19*, 4829.
(18) Miyashita, M.; Sunahara, K.; Nishikawa, T.; Uemura, Y.; Koumura, N.; Hara, K.; Mori, A.; Abe, T.; Suzuki, E.; Mori, S. *J. Am. Chem. Soc.* **2008**, *130*, 17874.
(19) Wang, Z-S.; Koumura, N.; Cui, Y.; Miyashita, M.; Furube, A.; Mori, S.; Hara, K. *Chem. Mater.* **2009**, *21*, 2810.
(20) Katoh, R.; Furube, A.; Mori, S.; Miyashita, M.; Sunahara, K.; Koumura, N.; Hara, K. *Energy Environ. Sci.* **2009**, *2*, 542.
(21) Hara, K.; Wang, Z-S.; Cui, Y.; Furube, A.; Koumura, N. *Energy Environ. Sci.* **2009**, *2*, 1109.

Polyaromatic Dyes for Dye-Sensitized Solar Cells

For a complete list of OPV dye materials, please visit *sigma-aldrich.com/opvdyes*

Name	Structure	Purity, Dye Content (%)	Spectroscopic Properties	Cat. No.
Anthracene		≥99%	-	694959-5G 694959-25G
Benz[*b*]anthracene		99.99% trace metals basis	λ_{max} = 277 nm, λ_{em} = 481, 514 nm in dichloromethane-d$_2$	698415-1G
Perylene		≥99.5%	λ_{max} = 436 nm, λ_{em} = 447 nm in tetrahydrofuran	394475-1G 394475-5G
4,4'-Bis(*N*-carbazolyl)-1,1'-biphenyl		≥99.99% trace metals basis	λ_{max} = 532 nm	699195-1G
N,*N*'-Di-[(1-naphthyl)-*N*,*N*'-diphenyl]-1,1'-biphenyl]-4,4'-diamine		99%	-	556696-500MG
Rubrene		-	λ_{max} = 299 nm, λ_{em} = 550 nm in tetrahydrofuran	551112-100MG 551112-500MG
Bathocuproine		99.99% trace metals basis	λ_{max} = 277 nm, λ_{em} = 386 nm in tetrahydrofuran	699152-500MG
1,3,6,8-Tetrabromopyrene		97%	-	717274-5G
1,3-Bis(*N*-carbazolyl)benzene		97%	λ_{max} = 292, 338 nm, λ_{em} = 345, 360 nm in tetrahydrofuran	701874-5G
2,5-Bis(1-naphthyl)-1,3,4-oxadiazole		99%	-	698202-5G
5,12-Dihydro-5,12-dimethylquino[2,3-*b*]acridine-7,14-dione		-	λ_{max} = 295 nm methylene chloride	557587-100MG 557587-500MG
3,5-Diphenyl-4-(1-naphthyl)-1*H*-1,2,4-triazole		97%	λ_{max} = 264 nm, λ_{em} = 367 nm in dichloromethane-d$_2$	703761-1G
Pyrene		99%	-	571245-1G
Merocyanine 540		Dye Content 90%	λ_{max} = 555 nm	323756-100MG 323756-250MG
Coumarin 6		≥99%	λ_{max} = 443 nm, λ_{em} = 505 nm in ethanol λ_{em} = 494 nm in tetrahydrofuran	546283-100MG
Coumarin 480 D		Dye Content 99%	λ_{max} = 392 nm, λ_{em} = 467 nm in ethanol	546232-100MG
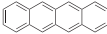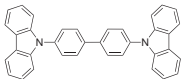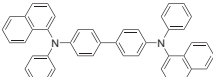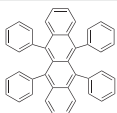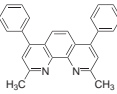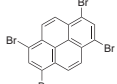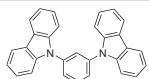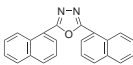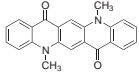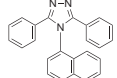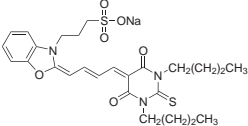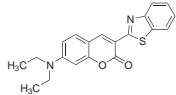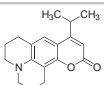
Name	Structure	Purity, Dye Content (%)	Spectroscopic Properties	Cat. No.
Coumarin 30		Dye Content 99%	λ_{max} = 413 nm, λ_{em} = 478 nm in ethanol	546127-100MG
Coumarin 153		Dye Content 98%	λ_{max} = 422 nm, λ_{em} = 532 nm in ethanol	546186-100MG
Coumarin 102		Dye Content 99%	λ_{max} = 390 nm, λ_{em} = 466 nm in ethanol	546151-100MG
Benzo[e]pyrene		99%	-	B10102-25MG B10102-100MG
9,10-Dihydrobenzo[a]pyr-ene-7(8H)-one		97%	-	180610-500MG 180610-1G
7-Methylbenzo[a]pyrene		98%	-	380903-100MG
1,3-Bis[4-(dimethylamino)phenyl]-2,4-dihydroxycyclo-butenediylium dihydroxide, bis(inner salt)		Dye Content 90%	λ_{max} = 625 nm	149063-1G

Photovoltaic Materials: Organic Semiconductors

The following tables list a selection of the available n-type and p-type semiconductor materials. For a complete list, please visit
sigma-aldrich.com/semiconductors

n-Type Semiconductors

Name	Structure	Purity (%)	Mobility	Absorption	Cat. No.
7,7,8,8-Tetracyanoquinodimethane		98	10^{-5} cm²/V·s	-	157635-5G 157635-10G
2,3,5,6-Tetrafluoro-7,7,8,8-tetracyanoquinodi-methane		97	-	-	376779-25MG 376779-100MG
1,4,5,8-Naphthalenetetracarboxylic dianhydride		-	0.003 cm²/V·s	-	N818-5G N818-25G N818-100G
Perylene-3,4,9,10-tetracarboxylic dianhydride		97	10^{-4} cm²/V·s	-	P11255-25G P11255-100G
N,N'-Dipentyl-3,4,9,10-perylenedicarboximide		98	~10^{-2} cm²/V·s	λ_{max} 527 nm	663921-500MG

Name	Structure	Purity (%)	Mobility	Absorption	Cat. No.
N,N′-Dioctyl-3,4,9,10-perylenedicarboximide		98	1.7 cm²/V·s	λ_{max} 526 nm	663913-1G
N,N′-Diphenyl-3,4,9,10-perylenedicarboximide		98	10^{-5} cm²/V·s	λ_{max} 527 nm	663905-500MG
5,10,15,20-Tetrakis(pentafluorophenyl)-21H,23H-porphine palladium(II)		-	-	λ_{max} 400 nm in acetone	673587-100MG
Copper(II) 1,2,3,4,8,9,10,11,15,16,17,18,22,23,24,25-hexade-cafluoro-29H,31H-phthalocyanine		-	-	λ_{max} 689 nm	446653-1G

p-Type Semiconductors

Name	Structure	Purity (%)	Cat. No.
5,5′′′′′-Dihexyl-2,2′:5′,2′′:5′′,2′′′:5′′′,2′′′′:5′′′′,2′′′′′-sexithiophene	$CH_3(CH_2)_4CH_2$ ... $CH_2(CH_2)_4CH_3$	-	633216-500MG
5,5′-Bis(2-hexyl-9H-fluoren-7-yl)-2,2′-bithiophene	$CH_3(CH_2)_4CH_2$ ... $CH_2(CH_2)_4CH_3$	-	703729-500MG
5,5′-Di(4-biphenylyl)-2,2′-bithiophene		97	695947-1G
3,3′′′-Didodecyl-2,2′:5′,2′′:5′′,2′′′−quaterthiophene	$CH_3(CH_2)_{10}CH_2$ / $CH_2(CH_2)_{10}CH_3$	97	691631-500MG
3,3′′′-Dihexyl-2,2′:5′,2′′:5′′,2′′′-quaterthiophene	C_6H_{13} / C_6H_{13}	95	694460-1G
α-Sexithiophene		-	594687-1G
2,2′:5′,2′′-Terthiophene		99	311073-1G
Dibenzotetrathiafulvalene		97	695637-500MG
Bis(ethylenedithio)tetrathiafulvalene		98	362026-500MG

For questions, product data, or new product suggestions, please contact Aldrich Materials Science at *matsci@sial.com*.

97

Photovoltaic Materials: ITO and Indium Oxide Powders

For a complete list of products, including ITO coated glass slides and PET sheets, please visit *sigma-aldrich.com/ito*

Name	Composition	Trace Metals Basis (%)	Physical Form	Particle Size	Cat. No.
Indium tin oxide	In_2O_3 90% / SnO_2 10%	≥99.99	-	−325 mesh	494682-25G 494682-100G
Indium tin oxide	In_2O_3 90% / SnO_2 10%	-	nanopowder	<50 nm	544876-5G 544876-25G
Indium tin oxide, dispersion	In_2O_3 90% / SnO_2 10%	-	30 wt. % in isopropanol, dispersion	<100 nm (DLS)	700460-25G 700460-100G
Indium(III) oxide	In_2O_3	99.999	powder	-	203424-5G 203424-25G
Indium(III) oxide	In_2O_3	99.99	powder	-	289418-10G 289418-50G
Indium(III) oxide	In_2O_3	99.9	nanopowder	<100 nm (BET)	632317-5G 632317-25G

Thiophene Building Blocks for Photovoltaic Materials Design

For a complete range of synthetic building blocks, please visit *sigma-aldrich.com/synthetic*

Name	Structure	Purity (%)	Cat. No.
2,5-Dibromo-3-butylthiophene		96	525499-1G 525499-5G
2,5-Dibromo-3-hexylthiophene		97	456373-1G 456373-5G
2,5-Dibromo-3-octylthiophene		96	525480-1G 525480-5G
2,5-Dibromo-3-decylthiophene		97	456381-1G 456381-5G
2,5-Dibromo-3-dodecylthiophene		97	456403-5G
2-Bromo-3-hexylthiophene		97	691925-1G 691925-5G
2-Bromo-3-dodecylthiophene		95	688312-1G
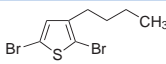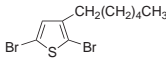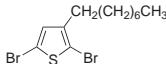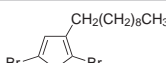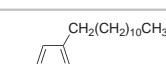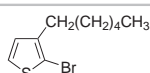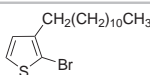
The Relentless Rise of Disruptive Photovoltaics

Scott Stephens
United States Department of Energy
Solar Energy Technologies Program
1000 Independence Ave., SW Washington, D.C., 20585
Email: scott.stephens@ee.doe.gov

Introduction

Continuous technological innovation has sustained over 30 years of cost reductions and exponential market expansion for photovoltaics. This article aims to provide a technological overview of the industry, to highlight some potential technology trends, and to convince the reader that this aggressive growth is likely to continue for the foreseeable future.

Market Growth

In 2008, the world market for Photovoltaics (PV) grew by 70% and resulted in approximately 6.9 gigawatts (GW$_p$) of manufacturing capacity which translates to nearly $40 Billion dollars worth of system-level newly added capacity. This growth is a continuation of the roughly 30% compound annual growth rate the industry has sustained for the past 30 years. Although the growth for 2009 is projected to be sharply lower and significantly negative in terms of revenue growth, the long-term growth prospects for the industry remain very promising primarily due to the potential of future cost reductions.

Technology Developments

Today, approximately 90% of cumulatively installed PV modules are based on crystalline silicon (c-Si) technology. The upstream manufacturing steps of this process are closely related to the standard wafering processes used in the integrated circuit industry, but with greater emphasis on throughput and feedstock efficiency. The process begins with "solar grade" polysilicon that typically is between 99.999% and 99.9999% pure, and in most cases containing fewer than 1 part per million (ppm) of boron and phosphorus, and less than 5 ppm total for all other metals. This polysilicon feedstock is cast into an ingot either by pulling a cylindrical single crystal from a melt or by freezing a multi-crystalline block in a ceramic crucible. The next step involves using a wire saw to slice the ingot into square wafers that are typically six inches in diameter and approximately 160-180 μm thick. Cell processing steps involve etching away the surface damage caused by the wire saw, diffusing either phosphorus or boron to form a pn junction, surface treatments to prevent charge carrier recombination and increase light capture, and applying metal contacts to collect the separated charge carriers. Today, there are numerous device architectures being manufactured, each with slight variations in this process and the addition of a few unique steps. Lastly, the finished cells are tiled, strung together (primarily in series to increase the voltage output), encapsulated between various polymer layers (the most common being one based on Ethylene-Vinyl Acetate or EVA on the front and a white back sheet often made of polyvinylfluoride), and encased with a front sheet of glass and supported along the edges with an aluminum frame. The final product (see Figure 1) is known as a panel or module, which is typically rectangular in shape, approximately 1-2 square meters in size with an output of around 150-250 watts at approximately 30-40 volts. Currently, most c-Si modules are rated to convert approximately 14-15% of incident light into electrical energy under standard testing conditions (25 °C, 1,000 W/m^2 energy incident on surface) although some manufacturers use advanced cell designs that allow modules efficiency ratings to approach 20%.
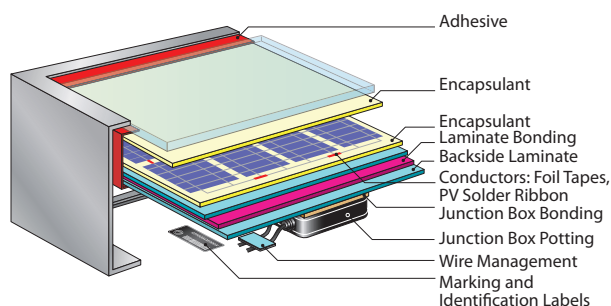
Figure 1. An exploded view of a typical rigid photovoltaic cell. Published with permission from Hisco.

Thin film modules offer an alternate approach that allows manufacturers to reduce material and processing costs. The three leading thin film technologies are based on amorphous or nanocrystalline silicon (a-Si, nc-Si), CdTe, and Cu(In,Ga)Se$_2$ (CIGS) as the light absorbing layer. PV cells are created by depositing submicron layers of these light absorbing direct bandgap materials onto a glass or metal foil substrate (Figure 2). Deposition techniques for the absorbing layer vary by technology type and include plasma-enhanced chemical vapor deposition for a-Si and nc-Si, close space sublimation or vapor phase transport for CdTe, and evaporation, sputtering, ink printing, or electroplating for CIGS. Other layers in thin film devices are deposited via sputtering or chemical bath. If all deposition steps achieve large area uniformity, the entire module can be deposited on a single large area substrate with cells formed via mechanical or laser etch steps, which is a process known as monolithic integration.
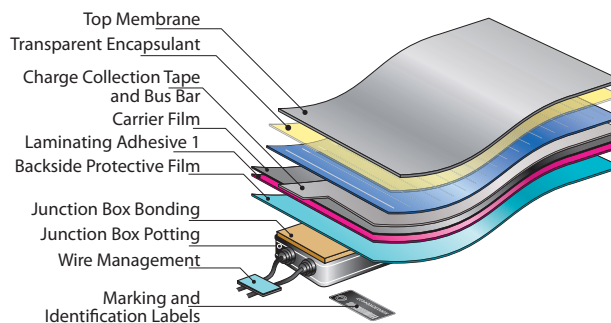
Figure 2. An exploded view of a typical flexible photovoltaic cell. Published with permission from Hisco.

For questions, product data, or new product suggestions, please contact Aldrich Materials Science at *matsci@sial.com*.

99

Concentrating PV (CPV) modules (**Figure 3**) reduce the impact of the high cost of semiconductors by shrinking the cell size and using an inexpensive optic to concentrate light onto a high performance cell. Concentration ratios range from 2-1,000 times the light produced by the sun, but are generally clustered around 3 ranges. Low concentration PV modules typically use c-Si cells, concentrate light approximately 1.5-3x, and are placed on a fixed mount that is optimally tilted for a given latitude. Mid-concentration ratios range from 5-30x with linear optics that focus light onto a row of high-performance c-Si cells. This linear configuration only requires tracking the azimuth (hour angle) motion of the sun that can allow lower costs.
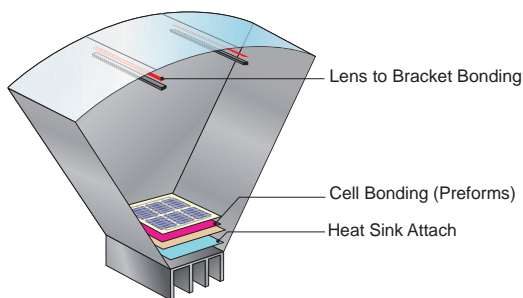
Figure 3. An exploded view of a typical CPV module with a Fresnel lens. Published with permission from Hisco.

High concentration PV generally ranges from 200-800x, requires 2-axis tracking, and uses very expensive yet highly efficient multijunction cells. High concentration is the most typical approach to CPV as the cell's cost contribution to the overall system price is minimized. Commercial multijunction cells currently approach 40% conversion efficiency and the 2-axis tracking allows modules to output more power in the early morning and late afternoon. However, there are also numerous drawbacks to CPV; additional costs and reliability concerns are incurred with the use of optics and a tracker, the cells only "see" a small region of the sky around the sun and so the diffuse component of the solar spectrum (~150 W/m^2) is lost, and most designs require each tracker to be sufficiently spaced to avoid shading.

Currently the U.S. Department of Energy's (DOE) Solar Energy Technologies Program ("Solar Program") funds research and product development efforts across all three of these general classifications of photovoltaics. Relative to the global energy industry, none of these PV technologies have achieved an efficient or significant manufacturing scale, and additionally, each of these technologies holds promise for disruptive or transformational improvements beyond what is currently considered state-of-the-art. Thus, current cost structures are not the best indicator of which photovoltaic technology is most promising in the >5 year timeframe. Furthermore, these technologies vary significantly in their performance with respect to parameters such as solar resource, temperature, power density, weight, modularity, etc. These differences are highlighted in **Figure 4** suggesting that there may be room in the market for multiple types of PV even as the industry matures. Existing product diversity in other technologies such as batteries or displays provides a strong precedent for such sustained market segmentation.
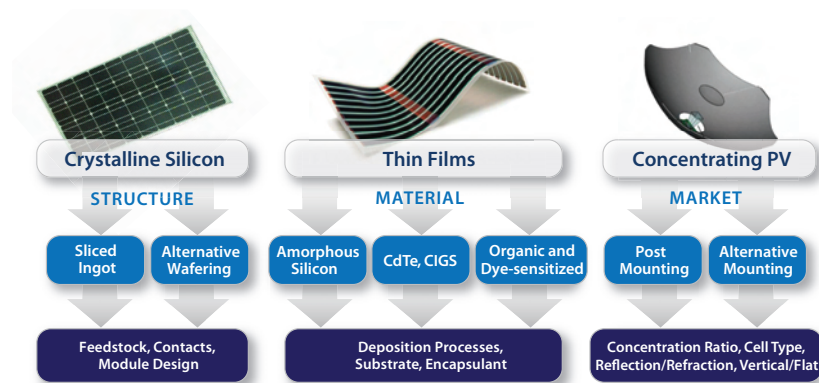
Figure 4. Significant differences in materials and processes exist across the three primary types of PV technologies. Differences in system attributes and performance across these technologies suggest that end markets may support multiple technology platforms into the future.

Since 2005, the Solar Program's stated goal for PV has been to achieve grid parity in residential, commercial, and utility markets and to install more than 5GW of peak capacity in the U.S. by 2015. These targets require a 50-70% reduction in levelized cost of electricity (LCOE) and a sustained 30% compound annual growth rate (CAGR) in the photo-voltaic industry's production relative to a 2005 baseline. LCOE is defined as the ratio of the net present value of a PV system's costs to its generated energy ($/kWh) over the life of the system. This equation, along with a non-exhaustive list of technology drivers of the LCOE, are shown in **Figure 5**.

$$LCOE = N.P.V. \frac{(price)}{(energy)} = \frac{\sum_{n=0}^{N} \frac{I_0 + M_n}{(1+d)^n}}{\sum_{n=0}^{N} \frac{Q_n}{(1+d)^n}}$$
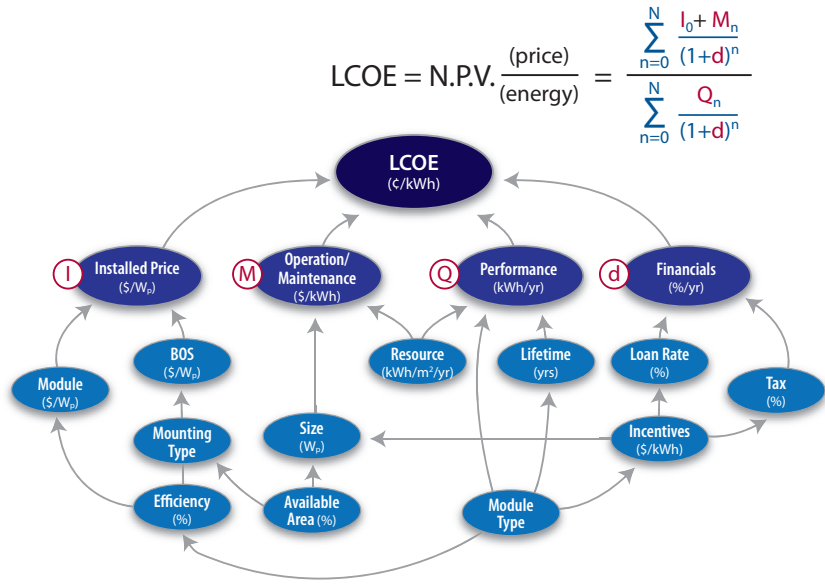
Figure 5. The Levelized Cost of Electricity (LCOE) is calculated from the Net Present Value (NPV) ratio of a system's price to its energy generation. A non-exhaustive list of significant LCOE drivers is shown along with their interdependencies.

Historically, as shown in **Figure 6**, modules have represented slightly more than 50% of an installed system price and thus were the focal point of the Solar Program's R&D program.
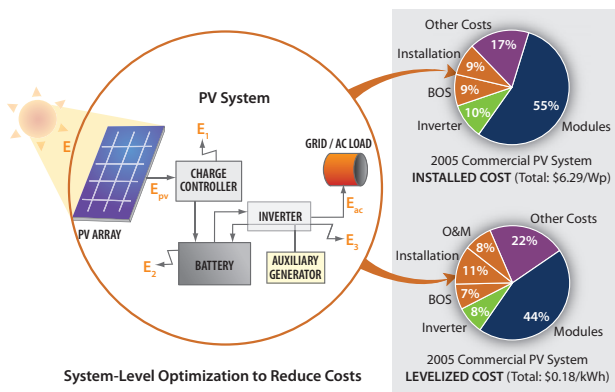
Figure 6. DOE's current PV research objectives target cost reductions at the system level.

Additionally, over 80% of the installed system costs scale directly with module efficiency. Until this decade, exploring ways to increase cell and module efficiency was the primary driver for advancing the technology. However, as cell efficiencies began to rise more slowly and PV systems became more competitive with grid-tied electricity, attention shifted to total installed system costs. Over the past three years, the DOE's Solar Program has shifted to a system-driven approach to address all significant LCOE drivers. In addition to module efficiency and cost, other key drivers include installation, labor costs, inverter lifetime, annual maintenance costs, and capital costs. A recent and continuing collapse in module prices has further justified this approach. Specific examples of these system cost drivers include; module level power conversion

(either DC-DC or DC-AC) that can reduce wiring costs, enable system design flexibility, and increase array shade tolerance. Reducing "fixed" system costs is achieved by moving to larger modules, higher voltages, or partially pre-assembled mounting structures, and improving system energy yield by using anti-soiling coatings or mounting high efficiency modules on inexpensive 1-axis trackers.

Future Promise

Moving forward, the PV industry appears poised for dramatic growth in the U.S. and worldwide. Over the past 30 years module prices have maintained a remarkably stable progress ratio of 80% as shown in **Figure 7**.
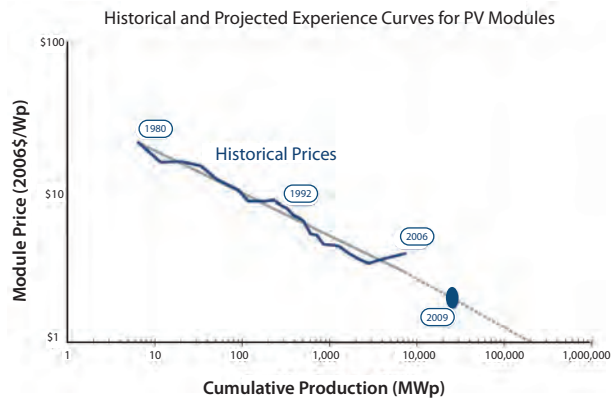
Figure 7. Historically, the price of PV modules has fallen by 20% for every doubling of cumulative production.

For questions, product data, or new product suggestions, please contact Aldrich Materials Science at *matsci@sial.com*.

101

ALDRICH Chemistry

Although there is less information available for installed system prices over this period, there are many reasons to expect a similar downward progression in total system price. The fundamental drivers for PV cost reduction are solar resources, technology, and market. Solar energy is the Earth's most abundant energy resource by a wide margin. Compared with other renewables, it is over ten times more abundant than wind, biomass, geothermal, tidal, and wave power combined. Compared with the world's current energy consumption, the amount of solar energy incident on the Earth is three orders of magnitude larger than the total world power demand. Moreover, it is more uniformly distributed across the Earth than any other energy source with most areas receiving several kWh worth of incident energy per square meter of land per day. In the past, this was critically important for the growth of PV as it enabled remote power production at a much cheaper price than building electrical transmission or transporting fuels. Today and into the future, this attribute remains important as this is roughly the power density required by most homes and buildings. Additionally, the distributed, grid-tied nature of PV generation fits within the constraints of the current transmission network, which is unable to move large amounts of power across long distances. The nature of PV technology promises continued cost reductions into the foreseeable future. The performance improvement and cost reduction of solid state photo-electric devices has, and continues to be, a result of technological and manufacturing improvements. Until recently, this was almost entirely due to the "learning by doing" improvements typical in all modular manufacturing of high tech products. This is likely to continue as the industry grows, but there is now greater attention being placed on lowering non-module costs by exploiting the modular nature of PV installations. Examples of this trend that go beyond traditional system design improvements include software-optimized system design and logistics management based upon standard rooftop or landscape drawings, developing automated installation equipment for ground mounted installations, or even integration of PV products with the manufacture of standard roofing products.

Finally, the abundant and distributed nature of the technology allows market penetration that is both incremental and non-uniform; these are requirements that any expensive, paradigm-shifting technology must conform to. In the mid 1990s, the number of newly added grid-tied solar installations surpassed off-grid systems in the world and marked the beginning of the technology's subtle entrance into the existing and enormous electricity market. Initially, the grid-tied market where PV is competitive with other available electricity was limited to regions with some combination of early adopters, strong incentives, progressive interconnection policy, low cost financing, high electricity rate, and to a lesser extent, a sunny climate. Over the past 15 years, prices have fallen as developments across all but the last of these market drivers have been strongly in favor of PV. There are a variety of reasons for these developments, but in general, they can be attributed to increased costs of traditional energy production and public support for an energy technology, which is inconspicuous, clean, and indigenous. Although cost remains the largest barrier to even greater adoption of PV, market barriers such as interconnection regulations and codes are increasingly a bottleneck. In the 5-15 year timeframe, the effect on the grid of PV's intermittent electricity production will need to be addressed as penetration levels pass 10-15% of the total local generation. It is important to note; however, that the production profile of PV is well correlated with most utility demand curves. In other words, photovoltaics produce power when utilities most need it. Thus, it is likely that promising developments such as smart grid technologies and distributive storage will significantly increase these penetration limits for distributive PV. In both the near and long term, the future for PV appears bright. Various industry experts have made analogies comparing the rise of the PV industry to the rapid growth in other technologies such as integrated circuits or flat panel displays. However, the low cost, long lifetime, and high volumes of materials and consumables associated with PV will ensure that the industry also bears some semblance to lower tech fields like roofing or windows. Ultimately, manufacturers and materials suppliers should anticipate some combination of these two development paths in order to harness the growth of this exciting industry.

Reference:
(1)   EERE Databook: http://www1.eere.energy.gov/maps_data/pdfs/eere_databook.pdf

High Purity Metal Selenides and Tellurides

For a complete list of materials for energy generation and storage, please visit *sigma-aldrich.com/renewable*

Name	Formula	Purity	Physical Form	Cat. No.
Zinc telluride	$ZnTe$	99.99% trace metals basis	−100 mesh, powder	254320-25G
Zinc selenide	$Zn=Se$	99.99% trace metals basis	10 µm, powder	244619-10G 244619-50G
Zinc selenide	$Zn=Se$	-	random pieces	553018-25G
Indium(III) telluride	In_2Te_3	99.999% trace metals basis	coarse powder	461016-5G 461016-25G
Copper(I) telluride	Cu_2Te	99.9% trace metals basis	crystalline	548472-25G
Copper(I) selenide	Cu_2Se	99.95% trace metals basis	powder and chunks	481629-5G
Cadmium zinc telluride	$CdZnTe$	99.99999% trace metals basis	pieces	716707-5G
Cadmium telluride	$CdTe$	≥99.99% trace metals basis	<250 µm, powder	256544-10G 256544-50G
Cadmium telluride	$CdTe$	99.99999% trace metals basis	pieces	716669-5G
Cadmium selenide	$CdSe$	99.99% trace metals basis	particle size ~10 µm, powder	244600-10G 244600-50G
Antimony(III) selenide	Sb_2Se_3	99.99% trace metals basis	solid	401196-5G

Ionic Liquids for Energy Storage Applications

John D. Stenger-Smith[1] and Jennifer A. Irvin[2]

[1]Naval Air Warfare Center, Weapons Division, China Lake, CA 93555
[2]Texas State University, San Marcos, TX 78666
Email: john.stenger-smith@navy.mil, jennifer.irvin@txstate.edu

Introduction

Ionic liquids, also called room temperature ionic liquids, are organic salts that are liquid at, or close to, room temperature. These salts (**Figure 1**) have been the subject of considerable interest due to their very low volatility and their ability to dissolve a wide variety of compounds; this combination of properties makes ionic liquids useful as "green" solvents for energy applications and industrial processes.
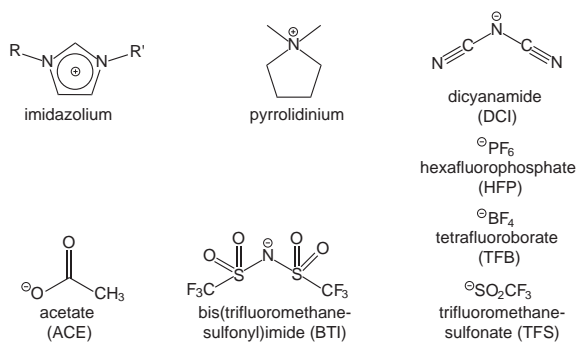
Figure 1. Common cations and anions found in ionic liquids

Another useful aspect of some ionic liquids is their broad window of electrochemical stability, which can be as large as 6.0 V.[1] This window makes these ionic liquids promising candidates for use as electrolytes for electrochemistry. While materials with large voltage windows are desirable, they may also possess unacceptably high viscosities and insufficient conductivities for use as electrolytes. High viscosities often result in higher oxidation potentials (due to decreased mass transport rates) and longer reaction times.[2] A perusal of some ionic liquid electrolytes (ILEs) shown in **Table 1** quickly reveals the trade-offs.

Table 1. Properties of some ionic liquids suitable for electrochemistry[1]

Ionic Liquid	M.P. (°C)	Viscosity (mm/s 25 °C)	Conduct. (mS/cm)	Electrochem. Window (V)
1-ethyl-3-methylimidazolium bis (trifluoromethylsulfonyl)imide (EMI-BTI) (**Aldrich Prod. No. 711691**)	-17	18	8.8	4.1
1-ethyl-3-methylimidazolium trifluoromethanesulfonate (EMI-TMS) (**Aldrich Prod. No. 711756**)	-9	43	9.2	4.1
1-butyl-1-methylpyrrolidinium bis (trifluoromethylsulfonyl)imide (BMP-BTI) (**Aldrich Prod. No. 38894**)	-50	71	2.2	5.5
1-hexyl-3-methylimidazolium hexafluorophosphate (HMI-HFP) (**Aldrich Prod. No. 89320**)	-80	548	1	5.5
1-ethyl-3-methylimidazolium dicyanamide (EMI-DCA) (**Aldrich Prod. No. 713384**)	-21	17	27	5.9
1-methyl-3-octylimidazolium tetrafluoroborate (MOI-TFB) (**Aldrich Prod. No. 96324**)	-88	422	0.43	6

A field that has seen significant benefits from the advent of ILEs is that of electroactive polymers. Electroactive polymers (EAPs) can generally be switched between two or more stable oxidation states, giving rise to changes in properties including conductivity, color, and volume. Color changes lead to electrochromic applications such as displays and auto-dimmable windows, while volume changes lead to electromechanical actuator applications such as artificial muscles and microelectrome-chanical devices (MEMs). Devices incorporating EAPs have been the focus of concentrated research for the past three decades. As these polymers have the possibility of being switched between their neutral forms, a p-type doped oxidized form, and an n-type doped reduced form, a variety of electrode configurations are possible. This has been exemplified by the use of electroactive polymers in electrochemical capacitors,[3] rechargeable storage batteries,[4] and electrochromic devices.[5] **Figure 2** shows the common oxidation and reduction reactions that occur with EAPs.
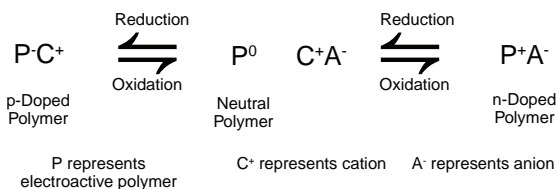
Figure 2. Generalized reaction scheme for an electroactive polymer (P) switching between n-doped, neutral, and p-doped states in the presence of an electrolyte (C⁺A⁻)

As shown in **Figure 2**, the oxidation, neutralization and reduction of EAPs require the movement of ions in order to obey conservation of charge. Ion choice can affect morphology, stability, and oxidation and reduction potentials.[6] Ions are introduced using electrolyte solutions such as tetraalkylammonium salts dissolved in water, acetonitrile or propylene carbonate (**Aldrich Prod. No. 310328**). The ionic liquids shown in **Figure 1** have attracted significant attention as alternative electrolytes for EAP-systems. They can be used in a pure form or in a combination with other solvents.[7-9] Advantages of ILEs include a broad temperature use window, low volatility, and good electrochemical and thermal stability.[10] When used without additional solvents, ionic liquid electrolytes significantly improve switching stability of EAP-based devices relative to solution based electrolytes.[11]

For questions, product data, or new product suggestions, please contact Aldrich Materials Science at *matsci@sial.com*.

103

Applications of Ionic Liquids in Supercapacitors and Batteries

Electrochemical Capacitors (Supercapacitors)

Electrochemical capacitors (ECs), also known as supercapacitors, are power leveling charge storage devices in which the oxidation and reduction of electroactive polymers, metal oxides, or carbonaceous materials are used to store electrical energy. In the charging process, the EC electrodes are reduced (cathode) and oxidized (anode) to store electrical energy, which is then released during discharge, as electrode materials return to their neutral states. **Figure 3** illustrates the generalized operation of a Type IV EC, which combines both p-doped (anode) and n-doped (cathode) polymers for maximum energy storage.
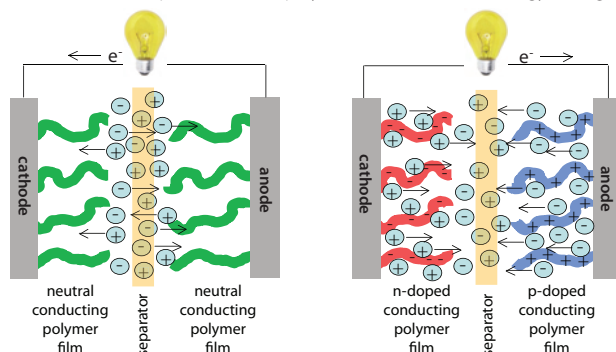
Figure 3. Electroactive polymer-based electrochemical capacitor schematic showing electron flow and ion movement during charge (left) and discharge (right). During charging, the polymer at the cathode (n-doped) becomes negatively charged, and cations from the electrolyte move in to compensate the charge. Simultaneously, the polymer at the anode (p-doped) becomes positively charged, and anions from the electrolyte move in to compensate the charge. During discharge, both polymers return to their neutral states, and ions return to the solution.

Among the most important applications of ECs are memory protection systems for portable electronics, load leveling for electric utilities and energy storage for electric vehicles. ECs generally provide more power per unit mass than batteries and store more energy per unit mass than traditional capacitors. Therefore, they may be used to supply burst power for electric vehicles. All ECs require an electrolyte for their operation; the use of ionic liquids[7,12] allows volatile and hazardous conventional solvents to be eliminated and improves the operational stability of these devices.

Lithium Ion Batteries

Li-ion batteries are ubiquitous in the consumer electronics market and may eventually dominate large-scale high power commercial energy storage. Lithium batteries are comprised of two lithium-intercalating oxide and carbon electrodes separated by an electrolyte (**Figure 4**). As the battery is charged, lithium ions move from the oxide electrode to the carbon electrode, storing energy. When the battery is discharged, the lithium ions move back to the oxide, and energy is released. Lithium ion transport is facilitated by an electrolyte, which typically contains a volatile, flammable solvent. Therefore, safety is a major concern in Li-batteries containing conventional electrolytes. Short circuits or local overheating in the presence of flammable solvents can cause thermal runaway, fire, and even explosion. Ionic liquids can be particularly helpful in lithium ion batteries, by replacing flammable solvents and improving battery safety.[10]
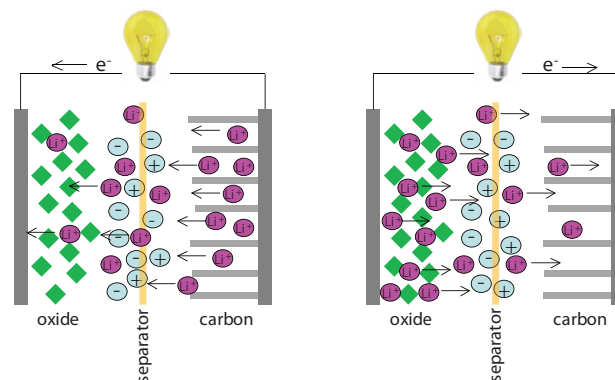
Figure 4. Lithium ion battery showing electron flow and lithium ion movement during discharge (left) and charge (right).

Furthermore, unlike electrochemical capacitor electrolytes, lithium battery electrolytes must facilitate the transport of lithium ions, remain stable at very negative potentials, and support stable operation of the battery. It is possible for ionic liquids to meet this requirement, and there are several research groups working in this area.[10,13] Among the ionic liquids that have been tested are *N*-butyl-*N*-ethyl pyrrolidinium bis(trifluoromethylsulfonylimide) (**Aldrich Prod. No. 38894**); ethylmethylimidazolium bis(trifluoromethylsulfonylimide) (**Aldrich Prod. No. 711691**); *N*-methyl-*N*-propyl pyrrolidinium bis(trifluoromethyl-sulfonylimide) and *N*-methyl-*N*-propyl piperidinium bis(trifluoromethyl-sulfonylimide). Any one of these could be used to prepare solutions of lithium bis(trifluoromethane sulfonylimide) (**Aldrich Prod. No. 544094**), where the lithium ion is the active material.

Ionic Liquids at Extreme Temperatures

With increasing focus on energy production and storage, there is a growing demand for charge storage devices that operate at a wide variety of temperatures. In the automotive industry, charge storage devices would ideally be operational at temperatures as low as -30 °C.[14] Military requirements for charge storage devices are even more severe, with temperatures as low as -60 °C targeted for some applications.[15] Most batteries suffer from severe performance degradation at lower temperatures, especially down to -60 °C.[16] Aside from slowing down the kinetics of the charge/discharge process, lower temperatures also increase the viscosity of electrolytes, reducing the ability of the electrolyte to transport charge. Such property changes lead to degradation of device performance or failure upon extended exposure to low temperatures. One of the most severe effects of low temper-atures on solution-based electrolytes is reduced solubility of the electrolyte material, resulting in precipitation of the salt and destruction of the electrochemical capacitor or battery. As evidenced from **Table 1**, many ionic liquid electrolytes are operational at the moderately low temperatures required by the automotive industry, but very few of those will function at the extremely low temperatures required for military applications.[17] Adding to the challenge is the fact that these electrolytes should support electrochemical processes (deposition, oxidation, reduction, device operation,[15] etc.) in a variety of monomer/polymer systems across the same broad temperature interval. Unfortunately, there are only a few ILEs that remain liquid at extremely low temperatures, and their viscosities may become prohibitively high for most of the electrochemical applications. Mixtures of different ionic liquids or the use of viscosity-reducing additives could help mitigate this problem. The performance of electrochemical devices at elevated temperatures up to 60 °C has also been of concern in the energy storage industry.[14] Unfortunately, most solvent-based electrolytes suffer from high solvent volatility at elevated temperatures. Solvent evapo-ration can result in fire and explosion in sealed systems; while in open systems, it may result in electrolyte precipitation, destruction of the charge storage materials, and loss of charge storage capability. Thus, the extremely low volatility of ionic liquids makes them excellent electro-lytes for use at elevated temperatures.

Other Applications

There are many other applications for which ionic liquids show potential. Wide electrochemical windows and low vapor pressures make them advantageous for electroplating metals and semiconductors.[18] Ionic liquids are also promising enabling technology for high-temperature fuel cells.[19] At temperatures exceeding 100 °C, when water as a solvent is not an option, ionic liquids offer an excellent alternative to conventional aqueous proton transfer systems. Electromechanical actuators utilizing electroactive or ion exchange polymers require an electrolyte to facilitate actuation; ionic liquids have been shown to enhance long term stability of these devices.[20] Perhaps the most prominent illustration of stability enhancement using ionic liquids are electrochromic devices, where no significant loss in electroactivity could be observed after 1,000,000 cycles when 1-butyl-3-methyl imidazolium tetrafluoroborate (**Aldrich Prod. No.** 711748) was used as the electrolyte in a polyaniline-based electrochromic display.[10]

Purity Requirements

Purity of the electrolytes used in energy storage applications is crucial for the stability and performance of electrochemical devices. Ionic liquids are no exception. Depending on the synthetic routes employed for the preparation of ionic liquids, impurities in these materials may include water, superfluous cations or anions, or other solvents. Even trace amounts of contaminants can result in undesirable side reactions and hamper the performance of EAP-based devices. Thus, chloride and water impurities have been shown to influence the viscosity of ionic liquids.[21, 22] Small amounts (a few ppm) of sorbents such as alumina and silica can also result in their reduced electrochemical performance.[23] Purification approaches that produce ionic liquids suitable for use in electrochemistry often involve column chromatography or vacuum distillation (to remove volatile impurities; the ionic liquids themselves do not distill). They have been published for many common materials and should be followed diligently.[21-23]

Summary and Conclusions

The very low volatility and good electrochemical stability of many ionic liquids make them an excellent choice for use as electrolytes in energy storage devices. For electrochemical applications, stringent purification is recommended. Excellent electrochemical stabilities are observed in devices utilizing ionic liquid electrolytes. The ability to operate at extreme temperatures is a unique feature of ionic liquid electrolytes, making them promising candidates for use in electric vehicles and many other applications.

Acknowledgments

References:
(1)   Galínski, M.; Lewandowski, A.; Stepniak, I. *Electrochim. Acta* **2006**, *51*, 5567.
(2)   Pringle, J. M.; MacFarlane, D. R.; Forsyth, M. *Synth. Met.* **2005**, *155*, 684.
(3)   Gottesfeld, S.; Ferraris, J. P.; Rudge, A.; Raistrick, I. *Electrochim. Acta* **1994**, *39*, 273.
(4)   Novák, P.; Müller, K.; Santhanam, K. S. V.; Haas, O. *Chem. Rev.* **1997**, *97*, 207.
(5)   Monk, P. M. S.; Mortimer, R. J.; Rosseinsky, D. R. *Electrochromism:Fundamentals and Applications*, VCH, Weinheim, **1995**.
(6)   Irvin, J. A.; Irvin, D. J.; Stenger-Smith, J. D. Electrically Active Polymers for Use in Batteries and Supercapacitors. in *Handbook of Conducting Polymers*, 3rd ed.; Skotheim, T., Ed.; Reynolds, J. R., Ed.; Taylor & Francis, Boca Raton, FL, **2008**.
(7)   Stenger-Smith, J. D.; Webber, C. K.; Anderson, N. A.; Chafin, A. P.; Zong, K.; Reynolds, J. R. *J. Electrochem. Soc.* **2002**, *149*, A973.
(8)   Pringle, J. M. *Polymer* **2005**, *46*, 2047.
(9)   Zakeeruddin, S. M.; Graetzel, M. *Adv. Funct. Mater.* **2009**, *19*(14), 2187.
(10) Armand, M.; Endres, F.; MacFarlane, D. R.; Ohno, H.; Scrosati, B. *Nature Mater.* **2009**, *8*, 621.
(11) Irvin, D. J.; Stenger-Smith, J. D.; Irvin, J. A. Electrochemical Supercapacitors Based on Poly(Xylyl Viologen) *Polymer Preprints* **2007**, *48*, 150.
(12) Balducci, A.; Henderson, W. A.; Mastragostino, M.; Passerini, S.; Simon, P.; Soavi, F. *Electrochim. Acta* **2005**, *50*, 2233.
(13) Matsumoto, H.; Sakebe, H.; Tatsumi, K. *J. Power Sources,* **2006**, *160*, 1308.
(14) Pesaran, A. A.; Markel, T.; Tataria, H. S.; Howell, D. "Battery Requirements for Plug-In Hybrid Electric Vehicles - Analysis and Rationale," Conference Paper July 2009 NREL/CP-540-42240.
(15) Department of Defense Test Method Standard MIL-STD-810G Method 502.5 (Low Temperature). http://www.dtc.army.mil/publications/MIL-STD-810G.pdf (accessed October 2009)
(16) Arbizzani, C.; Mastragostino, M.; Scrosati, B. in *Handbook of Conducting Polymers*, 2nd ed.; Skotheim, T. A., Ed.; Elsenbaumer, R. L., Ed.; Reynolds, J. R., Ed.; Marcel Dekker, NY **1998**.
(17) Aurbach, D. *Electrochim. Acta* **2004**, *50*, 247.
(18) Endres, F. *Electrodeposition from Ionic Liquids*, Abbott, A., Ed.; MacFarlane, D. R., Ed.; Wiley-VCH, Weinheim, Germany, **2008**.
(19) Greaves, T. L.; Drummond, C. J. *Chem. Rev.* **2008**, *108*, 206.
(20) Ding, J.; Zhou, D.; Spinks, G.; Wallace, G.; Forsyth, S.; Forsyth, M.; MacFarlane, D. *Chem. Mater.* **2003**, *15*, 2392.
(21) Seddon, K. R.; Stark, A.; Torres, M. J. *Pure Appl. Chem.* **2000**, *72*, 2275.
(22) Zhang, J.; Bond, A. M. *The Analyst* **2005**, *130*, 1132.
(23) Clare, B. R.; Bayley, P. M.; Best, A. S.; Forsyth, M.; MacFarlane, D. R. *Chem. Commun.* **2008**, 2689.

Ionic Liquids for Energy Applications

For a complete list of materials for energy generation and storage, please visit *sigma-aldrich.com/renewable*

Name	Structure	Purity (Assay) (%)	Melting Point (°C)	Cat. No.
1-Butyl-1-methylpyrrolidinium bis(trifluoromethylsulfonyl)imide		≥98.0	-18	38894-5G-F 38894-50G-F
Triethylsulfonium bis(trifluoromethylsulfonyl)imide		≥99.0	-35.5	08748-5G-F 08748-50G-F
1-Ethyl-3-methylimidazolium thiocyanate		≥99.0	-6	07424-5G-F 07424-50G-F
1-Butyl-2,3-dimethylimidazolium tetrafluoroborate		≥99.0	-	04383-5G-F 04383-50G-F
Methyl-trioctylammonium bis(trifluoromethylsulfonyl)imide		≥99	-	00797-5G-F 00797-50G-F
1-Ethyl-3-methylimidazolium tetrafluoroborate		≥99.0	15	00768-5G-F 00768-50G-F
1-Ethyl-2,3-dimethylimidazolium trifluoromethanesulfonate		≥99.0	-	00765-5G-F 00765-50G-F
1-Ethyl-3-methylimidazolium trifluoromethanesulfonate		≥99.0	-	00738-5G-F 00738-50G-F
1-Ethyl-3-methylimidazolium hexafluorophosphate		≥97.0	58-62	46093-5G-F 46093-50G-F
1-Butyl-4-methylpyridinium hexafluorophosphate		≥97.0	45	88458-5G 88458-50G
3-Methyl-1-propylpyridinium bis(trifluormethylsulfonyl)imide		≥97.0	0	30565-1G-F 30565-5G-F
1,3-Bis(cyanomethyl)imidazolium bis(trifluoromethylsulfonyl)imide		≥94	81-85	28961-5G-F 28961-25G-F
1-Methyl-3-(3,3,4,4,5,5,6,6,7,7,8,8,8-tridecafluorooctyl)imidazolium hexafluorophosphate		≥97.0	78-81	44979-1G-F

Name	Structure	Purity (Assay) (%)	Melting Point (°C)	Cat. No.
1-Ethyl-3-methylimidazolium bis(trifluoromethyl-sulfonyl)imide		≥97.0	−15	11291-1G-F 11291-5G-F
1,2-Dimethyl-3-propylimidazolium bis(trifluorome-thylsulfonyl)imide		≥97.0	15	50807-1G-F 50807-5G-F

Tetraalkyl Ammonium Salts for Electrochemistry

For a complete list of materials for energy generation and storage, please visit *sigma-aldrich.com/renewable*

Name	Structure	Purity (Assay) (%)	Melting Point (°C)	Cat. No.
Tetrabutylammonium bromide		≥99.0	102-106	86836-10G 86836-50G
Tetrabutylammonium iodide		≥99.0	141-143	86912-5G
Tetrabutylammonium perchlorate		≥99.0	211-215	86893-10G 86893-50G
Tetrabutylammonium tetrafluoroborate		≥99.0	155-161	86896-25G
Tetrabutylammonium tetraphenylborate		≥99.0	230-236	86897-5G
Tetrabutylphosphonium hexafluorophosphate		≥99.0	226-228	86927-5G
Tetrabutylphosphonium tetrafluoroborate		≥99.0	96-99	86934-25G
Tetraethylammonium chloride		≥99.0	-	86616-5G 86616-25G

Electroactive Polymers

For a complete list of electropolymers, please visit *sigma-aldrich.com/electropolymers*

Name	Structure	Description	Cat. No.
Poly[1,2-bis(ethylthio)acetylene]		average M_n ~1,200	446017-50MG
Poly(1,4-phenylene sulfide)		average M_n ~10,000	182354-5G 182354-100G 182354-250G
Poly(1,4-phenylene sulfide)		viscosity at 310 °C 275 poise	427268-100G
Poly(1,4-phenylene sulfide)		viscosity at 310 °C 500 poise	427241-100G 427241-500G
Poly(1,4-phenylene sulfide)		viscosity at 310 °C 1,400 poise	427233-100G
Polyaniline (emeraldine base)		average M_w ~5,000	556459-5G 556459-25G
Polyaniline (emeraldine base)		average M_w ~10,000	476706-10G 476706-50G
Polyaniline (emeraldine base)		average M_w ~20,000	556378-5G 556378-25G

For questions, product data, or new product suggestions, please contact Aldrich Materials Science at *matsci@sial.com*.

ALDRICH Chemistry

Name	Structure	Description	Cat. No.
Polyaniline (emeraldine base)		average M_w ~50,000	556386-5G 556386-25G
Polyaniline (emeraldine base)		average M_w ~65,000	530689-10G 530689-50G
Polyaniline (emeraldine base)		average M_w conductivity: ~100,000, 1×10^{-9} S/cm (pressed pellet, ASTM F8)	576379-5G 576379-25G
Polyaniline (emeraldine base)		average M_w ~300,000	576476-5G 576476-25G
Polyaniline (emeraldine salt)		conductivity: ~ 0.5 S/cm	577073-10G
Polyaniline (emeraldine salt)		conductivity: 30 S/cm	530565-5G 530565-25G
Polyaniline (emeraldine salt)		viscosity ~3 cP, conductivity: 10-20 S/cm	650013-10ML 650013-50ML
Polyaniline (emeraldine salt)		conductivity: ~ 1 S/cm	649996-10ML
Polypyrrole doped	• X organic acid anion	conductivity: > 0.0005 S/cm	482552-100ML
Polypyrrole	• X organic acid anion	conductivity: 0.8-1.0 S/cm	578177-10G
Polypyrrole	• X organic acid anion	conductivity: 10-40 S/cm	577030-5G 577030-25G
Polypyrrole	• X organic acid anion	conductivity: 30 S/cm	530573-25G
Polypyrrole	• X organic acid anion	conductivity: 13-20 S/cm	577065-10G

Polythiophenes

For a complete list of electropolymers, please visit *sigma-aldrich.com/electropolymers*

Name	Structure	Composition	Description	Additive	Cat. No.
Poly(3,4-ethylene-dioxythiophene)-*block*-poly(ethylene glycol) solution		1 wt % dispersion in nitromethane	conductivity: 0.5-3 S/cm, resistance 10,000-100,000 Ω/sq (spin cast thin films: typically 1-3 layers spun at 1,000 rpm) work function 4.33 eV 40 nm (RMS roughness spin cast thin films)	perchlorate	649805-25G
Poly(3,4-ethylene-dioxythiophene)-*block*-poly(ethylene glycol) solution		1 wt % dispersion in nitromethane	conductivity: 10^{-4}-10^{-3} S/cm, work function 4.19 eV	*p*-toluenesulfo-nate	649791-25G
Poly(3,4-ethylene-dioxythiophene)-*block*-poly(ethylene glycol) solution		1 wt % dispersion in propylene carbonate	0.5-3 S/cm (bulk)	perchlorate	649783-25G
Poly(3,4-ethylene-dioxythiophene), tet-ramethacrylate end-capped solution		0.5 wt. % (dispersion in propylene carbonate), Oligotron™ tetramethacry-late 0.5 wt. % propylene carbonate 99.5 wt. %	conductivity: 0.1-0.5 S/cm, resistance 1-10 M Ω/sq (typical surface resistance of film)	*p*-toluenesulfo-nate	649813-25G
Poly(3,4-ethylene-dioxythiophene), tet-ramethacrylate end-capped solution		0.5 wt. % (dispersion in nitromethane), Oligotron™ tetramethacry-late 0.5 wt. % ethanol 5.8 wt. % isopropanol 0.3 wt. % nitromethane 93.4 wt. %	conductivity: 0.1-0.5 S/cm, resistance 1-10 M Ω/sq (surface resistance of film)	*p*-toluenesulfo-nate	649821-25G
Poly(3,4-ethylene-dioxythiophene), bis-poly(ethyleneglycol), lauryl terminated		0.4-0.9 wt. % (content of dispersion), Acetonitrile 4-8 wt. % Aedotron™- C3 polymer 0.2-0.7 wt. % Nitromethane 90-95 wt. % Propylene glycol 0.0-0.3 wt. % proprietary processing additive 0.1-0.7 wt. %	conductivity: 10-60 S/cm, surface resistivity 600-3000 Ω/sq	-	687316-25G

For questions, product data, or new product suggestions, please contact Aldrich Materials Science at *matsci@sial.com*.

109

High-Tech Carbons

Engineered for Applications on This World and Beyond

The Sigma-Aldrich® commitment to carbon materials research and product development spans more than two decades. Understanding how thermodynamic and kinetic properties affect performance characteristics of both existing and novel carbons is our primary focus. The knowledge gained from this fundamental research has led to innovative new carbons and subsequent advances in the performance of many others. Today, we offer over 45 different carbons ranging in particle size from <0.2 to 841 μm and surface areas from 5 to 1,500 m²/g.

The unique and valuable characteristics of our carbon materials warranted their inclusion in experiments onboard the 1995 Galileo Mission to Jupiter, the 2005 Cassini-Huygens Missions to Saturn's largest moon Titan, and the 2007 Phoenix Mission to Mars.

An important area of rapidly growing interest is the use of mesoporous and high surface area carbons in supercapacitor research. A list of selected Sigma-Aldrich carbon materials and their physical characteristics are shown in the **Table 1.** For a complete list of our materials for energy applications, visit *sigma-aldrich.com/renewable*.

Table 1. High surface area carbons

Prod. No.	Carbon	Surface Area (m²/g)	Pore Volume (cc/g)			Pore Diameter (Å)	Particle Size		Pkg Size (g)
			Micro	Meso	Macro		Mesh	μm	
699624-5G	Mesoporous carbon, graphitized	70				137		<0.5	5
699640-5G	Mesoporous carbon	203	-	0.49	-	96.3	-	40-50	5
699632-5G	Mesoporous carbon, purified	214	0.06	0.28	-	63.9	-	<0.2	5
11051-U	Carbopack™ Z	220	-	1.73	-	255	60/80	177-250	10
10439-U	Carbopack X	240	-	0.62	-	100	120/400	37-125	50
10264	Carboxen™ 564	400	0.24	0.13	0.14	6-9	20/45	354-841	10
10269	Carboxen 569	485	0.20	0.14	0.10	5-8	20/45	354-841	10
10263	Carboxen 563	510	0.24	0.15	0.24	7-10	20/45	354-841	10
10184	Carbosieve™ S-III	975	0.35	0.04	-	4-11	60/80	177-250	10
10471	Carboxen 1003	1,000	0.38	0.26	0.28	5-8	40/60	250-400	10
10190-U	Carbosieve S-II	1,059	0.45	0.01	-	6-15	80/100	149-177	10
11072-U	Carboxen 572	1,100	0.41	0.19	0.24	10-12	20/45	354-841	10
10199	Carbosieve G	1,160	0.49	0.02	-	6-15	80/100	149-177	5
11052-U	Carboxen 1000	1,200	0.44	0.16	0.25	10-12	80/100	149-177	100

For additional information on these, or any other products, contact **matsci@sial.com**

Selected Applications of Metal-Organic Frameworks in Sustainable Energy Technologies
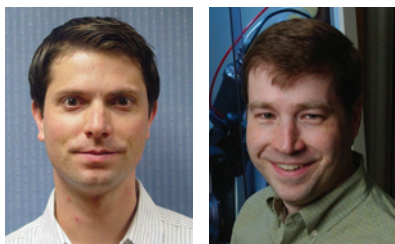
Stephen R. Caskey[1] and Adam J. Matzger[2]
[1]Sigma-Aldrich Corp., Milwaukee, WI 53209
[2]Department of Chemistry and the Macromolecular Science and Engineering Program, University of Michigan, Ann Arbor, MI 48109
Email: stephen.caskey@sial.com, matzger@umich.edu

Introduction

Although the field of high surface area materials is considered very mature, the need for improved materials for alternative energy applications remains pressing. Currently, zeolites, metal oxides, and activated carbons dominate the market, but more advanced materials are required for a variety of applications.[1] A potential solution has come from a somewhat unlikely place: coordination polymers. Although extremely well-studied for decades, the types of metal-ligand inter-actions that can reliably yield permanently porous coordination networks only emerged approximately ten years ago. This happened after the discovery of metal-organic materials having higher surface areas than the best zeolites. The term metal-organic frameworks (MOFs) has been used extensively to describe such coordination polymers. Further developments of MOFs has led to materials with record-setting surface areas, surpassing the best activated carbons.[2-4] The surface area of one gram of some MOFs approach that of a football field (120 x 53.33 yards implies 6,400 sq. yards or ca. 5,351 m^2).
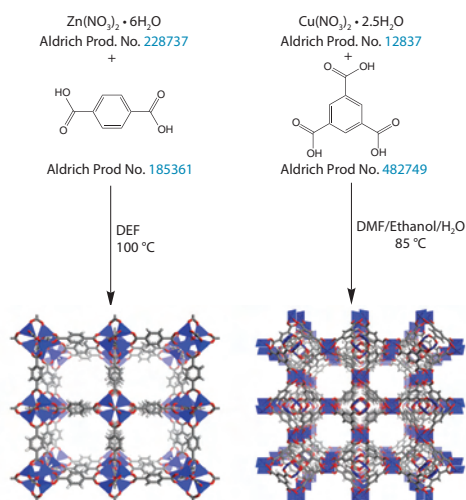
Figure 1. Typical approach to the synthesis of MOFs

The two most examined MOFs, known as MOF-5[5] and HKUST-1 (Hong Kong University of Science and Technology) also called Cu-BTC,[6] were first reported in 1999. MOF-5 is composed of zinc(II) clusters with terephthalic acid dianion as the organic linker as depicted in **Figure 1**. The Brunauer-Emmett-Teller (BET) surface area of MOF-5, which accounts for the possibility of multilayer gas adsorption on a surface, is ca. 3,500 m^2/g. HKUST-1 is composed of copper(II) paddlewheel dimers linked by trimesic acid trianion (**Figure 1**). The surface area of HKUST-1 (commercially available as Basolite C 300 under **Aldrich Prod. No. 688614**) is ca. 1,900 m^2/g. MOF-177, which is among the highest known surface area materials, is the prototypical high performance MOF (**Figure 2**).[7] The metal cluster in MOF-177 is the same as that of MOF-5. However, unlike MOF-5, the linker is not linear but rather derived from the tritopic carboxylic acid 1,3,5-tris(4'-carboxyphenyl)benzene, often referred to as H_3BTB (**Aldrich Prod. No. 686859**). MOF-177 is formed under identical conditions as MOF-5 (*N*,*N*-diethylformamide, 100 ºC). Its BET surface area approaches 4,750 m^2/g.[8]
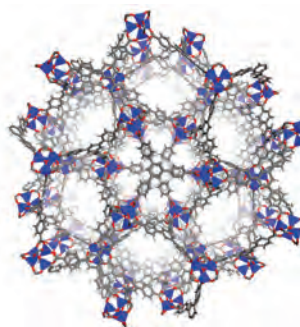
Figure 2. Crystal structure diagrams of MOF-177.

The Chemistry of MOFs

As a rule, MOFs are synthesized under solvo- or hydrothermal conditions in the presence of a base. A typical synthetic scheme is depicted in **Figure 1**. Many MOFs are prepared in pure *N*,*N*-diethylformamide (DEF, **Aldrich Prod. No. 186317**) or *N*,*N*-dimethylformamide (DMF, **Aldrich Prod. No. 227056**), which are well known to undergo decomposition at elevated temperatures to slowly generate an amine base that deprotonates the organic functionalities of the linker and generates the metal-organic clusters. The reactions are carried out either in glass scintillation vials (ca. 100 mg) or in glass jars (1-10 g) sealed with Teflon-lined caps to prevent solvent escape and/or corrosion of the caps. The reaction solutions are then heated to 50-250 ºC and crystalline materials are thus formed. Subsequently, the solvent is removed from the crystals. The crystals are submerged in a variety of low boiling, non- or weakly coordinating solvents (such as $CHCl_3$, CH_2Cl_2, methanol, ether) to extract DEF, DMF, and/or water from the pores of the material. Finally, the crystals are filtered from the solution and dried under vacuum at elevated temperature to completely evacuate the pores. Once the MOF is evacuated it is likely to become air and moisture-sensitive, i.e., it may decompose or re-hydrate irreversibly in air. Some tips for maximizing the surface area of a MOF include using fresh DEF or DMF (which tend to degrade over time or upon exposure to air), filtration and/or sonication of the reaction mixture prior to heating, degassing of the reaction solvent with N_2, and certainly the proper activation/evacuation procedure described above. Each of these steps can reduce crystal defects and enhance the surface area of the material. The most important analytical techniques used in the characterization of new materials include surface area analysis by gas sorption, X-ray diffraction (XRD powder and/or single crystal), elemental microanalysis (CHN), IR, and thermogravimetric analysis (TGA). Each freshly prepared batch of a known MOF should be characterized by XRD and surface area analysis to confirm its phase purity. Often, however, the presence of inter-penetration, i.e., another framework within the pores of the first framework, is difficult to detect. Such additional framework may have a profound effect on properties of the material through pore blockage.[9]

For questions, product data, or new product suggestions, please contact Aldrich Materials Science at *matsci@sial.com*.

111

Tools for designing high-performance MOFs, metal salts (nitrates) and solvents are nowadays commercially available. Linkers suitable for the synthesis of MOF-177[7] (**Aldrich Prod. No. 686859**), UMCM-150[10] (**Aldrich Prod. No. 714747**), mesoMOF-1[11] (**Aldrich Prod. No. 719250**), NOTT-101[12] (**Aldrich Prod. No. 716502**), and other well-known structures, which can be used as reference materials or in the development of new MOFs are also commercially available (**Figure 3**).

Aldrich Prod. No. 686859

Aldrich Prod. No. 706884

Aldrich Prod. No. 719250

Aldrich Prod. No. 714747

Aldrich Prod. No. 716502

Aldrich Prod. No. 715298

Aldrich Prod. No. 717312
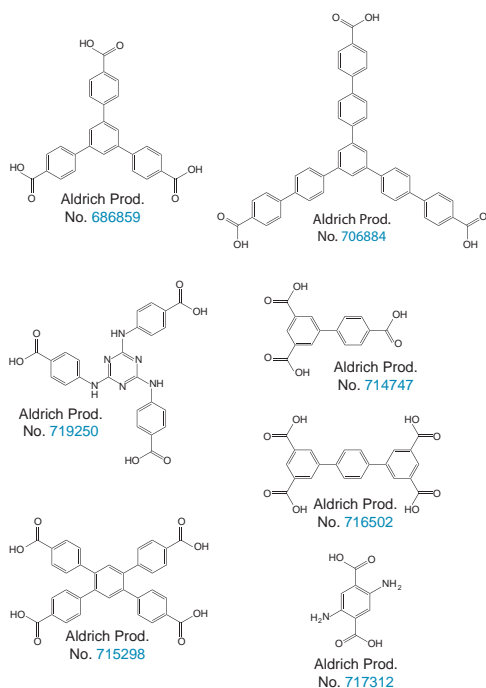
Figure 3. Some linker molecules for high performance MOFs available through Aldrich.

Applications

By far, the most widely examined use for MOFs is gas storage toward alternative, clean mobile energy. Two of the main candidates being examined include hydrogen gas and methane gas. Hydrogen certainly represents the cleaner (greener) option but the difficulty of producing, safely storing, and transporting hydrogen in large quantities has limited its utility to date. Hydrogen is attractive due to the high energy output with low environmental effect since water is its combustion by-product. Transport of hydrogen represents a significant challenge due to its low molecular weight and very weak attractive forces between hydrogen molecules. The storage for hydrogen in a given space at a given temperature and pressure can be increased by physisorptive binding of hydrogen to a surface, which enables closer packing of its molecules by weakly attractive forces. MOFs, as the highest surface area materials known, represent the best opportunity to meet these requirements. Separation and purification applications represent further opportunities for MOFs. Often, energy-intensive processes, such as distillation or conversion of one component into something more easily removeable, are used to achieve difficult separations. Simplifying these processes could mean significant savings of energy resources. Therefore, in the context of energy applications, the separation of CO_2 from flue gas using MOFs will be discussed in our article below.

Hydrogen Storage

Although initial reports of high levels of room temperature hydrogen storage in MOFs generated much interest, the failure to reproduce these initial results has led to a shift towards cryogenic storage. Cryogenic hydrogen storage has now been studied in a variety of MOFs,[13]

including MOF-177, which was shown to reversibly uptake 7.5 wt % hydrogen at 77 K (-196 °C) and ca. 55 bar. **Figure 4** illustrates MOF-177's superiority over other MOFs in terms of high-pressure hydrogen storage.[8] Although this result remains far from the DOE YR2015 goal of 7.5% for a storage system,[14] it still represents among the highest excess hydrogen uptake for a physisorptive material. Higher surface area MOFs generally trend toward higher hydrogen storage capacity, but it cannot be assumed that a high surface area always implies higher capacity, as shown in the case of UMCM-2.[3] The BET surface area of this MOF is 5,200 m^2/g, the highest of all published materials, yet the excess gravimetric hydrogen uptake at 6.9 wt % for UMCM-2 still falls short of that for MOF-177. This could be related to pore volume, pore shape, and/or other features that have not yet been fully recognized in MOFs. Thus, there remain considerable challenges and opportunities to rationally increase hydrogen storage capacity in MOFs beyond their current levels.
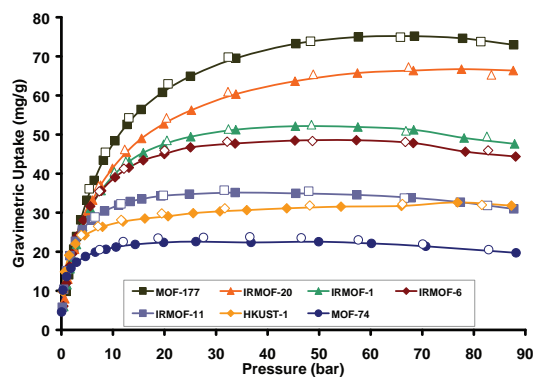
Figure 4. Hydrogen storage in different MOFs. Adsorption data are shown as closed circles, desorption data as open circles. Reprinted with permission from the American Chemical Society.

A large amount of research has focused on increasing the affinity of MOFs for hydrogen while maintaining high surface area and the reversibility of adsorption and desorption. To do this would entail increasing the heat of hydrogen adsorption. The factors that govern the heat of adsorption are poorly understood for physisorptive materials, but it is speculated that they may include the incorporation of small pores, pore shape (cylindrical vs. rectangular, etc.), and coordinatively unsaturated metal centers, each of which could promote tight binding of hydrogen. Until recently, MOF-505, a Cu-based MOF formed from biphenyl-3,5,3',5'-tetracarboxylic acid, has been cited as being the highest capacity, low pressure hydrogen uptake material (2.6 wt %) at 77 K and 1 atm, which indicates its high heat of hydrogen adsorption and a strong hydrogen affinity.[15] UMCM-150, another Cu-based material, has a lower heat of adsorption for hydrogen at 7.3 kJ/mol. However, it still displays impressive excess gravimetric hydrogen uptake of 2.1 wt % at 77 K and 1 bar due to significantly higher surface area than MOF-505.[10] MOF-74 and Co-, Ni-, and Mg-based analogs,[16] which are all formed using 2,5-dihydroxyterephthalic acid (**Aldrich Prod. No. 382132**), have small cylindrical pores with coordinatively unsaturated metal centers. They are also known to have high heats of adsorption for hydrogen at 77 K and 1 atm.[17,18] These MOFs are generally limited by relatively low surface areas, though.[8] Hupp and coworkers have used post-synthetic modification of a Zn-based 1,2,4,5-tetrakis(4'-carboxy-phenyl)benzene (**Aldrich Prod. No. 715298**), 3-di(4-pyridyl)-2,3-butane-diol (**Aldrich Prod. No. 43653**) pillared MOF with lithium or magnesium ions to increase affinity and uptake of hydrogen. Unfortunately, their material demonstrated only low surface areas of (ca. 800 m^2/g).[19]

It should be noted that increasing hydrogen affinity in the low pressure regime may ultimately have limited value. The operating pressure for a storage system is unlikely to be less than 1 atm, meaning that uptake below this pressure is essentially wasted on gas that can not be delivered.

Methane Storage

Compressed natural gas (CNG) vehicles are already on the road today. Gas (methane) pressures in the fuel tank of such vehicles can approach 3,600 psi (248 bar). To reach similar economical energy output, yet improve safe storage and transport, the DOE has set targets for methane storage of 180 v(STP)/v (v(STP) = standard temperature and pressure of methane; v = volume of adsorbent) under 35 bar.[20] A number of MOFs in the IRMOF series,[21] i.e., Zn-based MOFs with the same metal cluster but varying linear organic linkers, were tested for methane storage. IRMOF-6 (155 cm^3(STP)/cm^3) was found to be the highest in this series surpassing MOF-5 (135 cm^3(STP)/cm^3) and IRMOF-3 (120 cm^3(STP)/cm^3) at 36 atm. Examination of the Raman spectra of the adsorbed methane at pressures of up to 30 bar in the IRMOF series revealed that variation in the organic linker alone can significantly influence the adsorption affinity of methane in these materials.[22] Zhou has recently reported that a Cu-MOF, PCN-14, with an anthracene-based linker can demonstrate high uptake of methane (absolute methane adsorption capacity estimated to be 230 v/v at 35 bar and 290 K).[20] Although an impressive accomplishment, some doubt has been expressed that this has in fact exceeded the DOE target, based, in part, on the difference between a crystallographic density and a bulk packing density.[23]
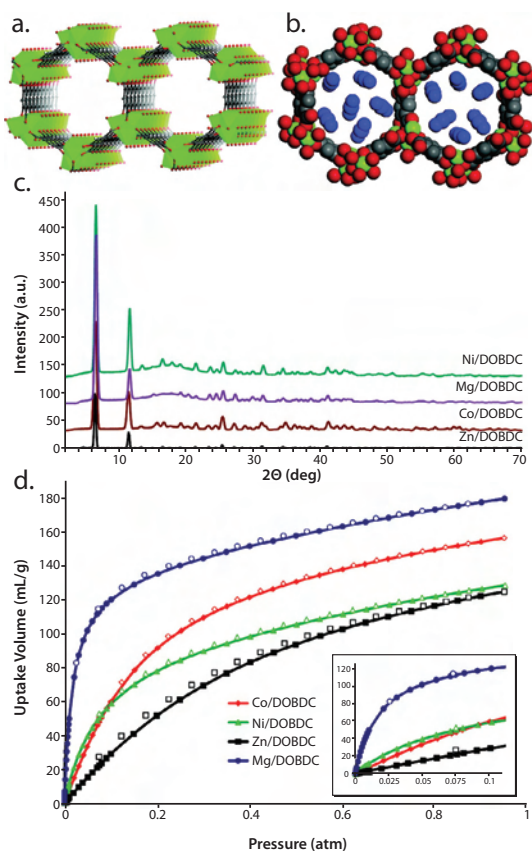
Figure 5. a) Structure of MOF-74 analogs b) Structure of MOF-74 analogs containing CO_2 colecules c) Powder x-ray patterns of MOF-74 analogs d) Low-pressure carbon dioxide adsorption for analogs of MOF-74 (Co^{II}, Ni^{II}, Mg^{II}, and Zn^{II}). Reprinted with permission from the American Chemical Society.

Carbon Dioxide Capture

Even with the global push for alternative energy, carbon dioxide emission remains a growing concern. For example, if methane gas were implemented as a primary fuel source, CO_2 would still be emitted as a by-product of combustion. Currently the largest single point sources of

CO_2 emission are power plants that produce streams of flue gas, exhausted combustion smoke, with CO_2 concentrations of ca. 15% at 1 atm. While storage of CO_2 is not much of a challenge, the separation of CO_2 from streams of flue gas represents a significant problem that must be addressed by the development of high CO_2 affinity materials before any thought of geologic sequestration can be effectively implemented. We recently published data on the use of MOF-74, a Zn-based material, and its Co-, Ni-, and Mg-based analogs in the uptake of CO_2 at low pressure.[16] The Mg-based analog of MOF-74 (Mg/DOBDC) was found to uptake ca. 35 wt % CO_2 at 1 atm and RT (**Figure 5**). This value is significantly higher than that of any other physisorptive material under the same conditions including zeolite 13X (molecular sieve type 13X). Since our report, Blom, Dietzel, and co-workers have confirmed our results and reported an X-ray crystal structure data showing CO_2 molecules bound to the metal centers in the Ni-based analog of MOF-74.[24] Accomplishing such uptakes in the presence of other components in flue gas is ultimately needed to contemplate replacing existing capture technologies based on chemisorption by amines.

Summary

Metal-organic frameworks, a subset of coordination polymers, represent a powerful new tool for a plethora of alternative energy applications. MOFs are readily available using simple synthetic strategies that supply tailored, high surface area materials. Current MOF technology sets the standard for cryogenic and room temperature storage of hydrogen and methane, respectively. Furthermore, new opportunities in separations using MOFs provide the prospect of clean, alternative energy capabilities.

References:
(1) For a review issue regarding MOF applications see: *Chem. Soc. Rev.* **2009**, *38*, 1201.
(2) Koh, K.; Wong-Foy, A. G.; Matzger, A. J. *Angew. Chem., Int. Ed.* **2008**, *47*, 677, and references therein.
(3) Koh, K.; Wong-Foy, A. G.; Matzger, A. J. *J. Am. Chem. Soc.* **2009**, *131*, 4184.
(4) Wang, Z.; Tanabe, K. K.; Cohen, S. M. *Inorg. Chem.* **2009**, *48*, 296.
(5) Li, H.; Eddauoddi, M.; O'Keeffe, M.; Yaghi, O. M. *Nature* **1999**, *402*, 276.
(6) Chui, S. S.-Y.; Lo, S. M.-F.; Charmant, J. P. H.; Orpen, A. G.; Williams, I. D. *Science* **1999**, *283*, 1148.
(7) Chae, H. K.; Siberio-Pérez, D. Y.; Kim, J.; Go, Y.; Eddaoudi, M.; Matzger, A. J.; O'Keeffe, M.; Yaghi, O. M. *Nature* **2004**, *427*, 523.
(8) Wong-Foy, A. G.; Matzger, A. J.; Yaghi, O. M. *J. Am. Chem. Soc.* **2006**, *128*, 3494.
(9) Hafizovic, J.; Bjørgen, M.; Olsbye, U.; Dietzel, P. D. C.; Bordiga, S.; Prestipino, C.; Lamberti, C.; Lillerud, K. P. *J. Am. Chem. Soc.* **2007**, *129*, 3612.
(10) Wong-Foy, A. G.; Lebel, O.; Matzger, A. J. *J. Am. Chem. Soc.* **2007**, *129*, 15740.
(11) Wang, X.-S.; Ma, S.; Sun, D.; Parkin, S.; Zhou, H.-C. *J. Am. Chem. Soc.* **2006**, *128*, 16474.
(12) Lin, X.; Telepeni, I.; Blake, A. J.; Dailly, A.; Brown, C. M.; Simmons, J. M.; Zoppi, M.; Walker, G. S.; Thomas, K. M.; Mays, T. J.; Hubberstey, P.; Champness, N. R.; Schröder, M. *J. Am. Chem. Soc.* **2009**, *131*, 2159.
(13) Murray, L. J.; Dinca, M.; Long, J. R. *Chem. Soc. Rev.* **2009**, *38*, 1294.
(14) Department of Energy, *DOE Targets for On-Board Hydrogen Storage Systems for Light-Duty Vehicles*, http://www1.eere.energy.gov/hydrogenandfuelcells/storage/pdfs/targets_onboard_hydro_storage.pdf.
(15) Chen, B.; Ockwing, N. W.; Millward, A. R.; Contreras, D. S.; Yaghi, O. M. *Angew. Chem. Int. Ed.* **2005**, *44*, 4745.
(16) Caskey, S. R.; Wong-Foy, A. G.; Matzger, A. J. *J. Am. Chem. Soc.* **2008**, *130*, 10870, and references therein.
(17) Liu, Y.; Kabbour, H.; Brown, C. M.; Neumann, D. A.; Ahn, C. C. *Langmuir* **2008**, *24*, 4772.
(18) Zhou, W.; Wu, H.; Yildirim, T. *J. Am. Chem. Soc.* **2008**, *130*, 15268.
(19) Mulfort, K. L.; Farha, O. K.; Stern, C. L.; Sarjeant, A. A.; Hupp, J. T. *J. Am. Chem. Soc.* **2009**, *131*, 3866.
(20) Ma, S.; Sun, D.; Simmons, J. M.; Collier, C. D.; Yuan, D.; Zhou, H.-C. *J. Am. Chem. Soc.* **2008**, *130*, 1012.
(21) Eddaoudi, M.; Kim, J.; Rosi, N.; Vodak, D.; Wachter, J.; O'Keeffe, M.; Yaghi, O. M. *Science* **2002**, *295*, 469.
(22) Siberio-Pérez, D. Y.; Wong-Foy, A. G.; Yaghi, O. M.; Matzger, A. J. *Chem. Mater.* **2007**, *19*, 3681.
(23) Sun, Y.; Liu, C.; Su, W.; Zhou, Y.; Zhou, L. *Adsorption* **2009**, *15*, 133.
(24) Dietzel, P. D. C.; Johnsen, R. E.; Fjellvåg, H.; Bordiga, S.; Groppo, E.; Chavan, S.; Blom, R. *Chem. Commun.* **2008**, 5125.

For questions, product data, or new product suggestions, please contact Aldrich Materials Science at *matsci@sial.com*.

113

Organic Linker Molecules for Metal-Organic Frameworks

For a complete list of organic linker molecules for MOFs, please visit *sigma-aldrich.com/moflinker*

Name	Structure	Purity (Assay) (%)	Cat. No.
4,4′,4″-(1,3,5-Triazine-2,4,6-triyltriimino)trisbenzoic acid		>95	719250
[1,1′:4′,1″:4″,1‴]Quaterphenyl-3,3‴,5,5‴-tetracarboxylic acid		>95	716499
2,5-Diaminoterephthalic acid		>95	717312-500MG
1,2,4,5-Tetrakis(4-carboxyphenyl)benzene		≥98	715298-1G
[1,1′:4′,1″]Terphenyl- 3,3″,5,5″-tetracarboxylic acid		>95	716502-500MG
Biphenyl-3,4′,5-tricarboxylic acid		>95	714747-500MG
1,3,5-Tris(4′-carboxy[1,1′-biphenyl]-4-yl)benzene		95	706884-500MG
1,3,5-Tris(4-carboxyphenyl)benzene		≥98	686859-1G
2,5-Dihydroxyterephthalic acid		98	382132-5G 382132-25G
2,6-Naphthalenedicarboxylic acid		99	523763-5G
2-Methylimidazole		99	M50850-100G M50850-500G
Imidazole		99	I202-1G I202-5G I202-100G I202-500G I202-2KG
Terephthalic acid		98	185361-5G 185361-100G 185361-500G
Trimesic acid		95	482749-100G 482749-500G

Selected Metal Salts for Synthesis of Metal-Organic Frameworks

For a complete list of metal salts and other related materials, please visit *sigma-aldrich.com/ceramics*

Name	Structure	Purity (Trace Metal Basis) (%)	Cat. No.
Zinc nitrate hydrate	$Zn(NO_3)_2 \cdot 6H_2O$	99.999	230006-25G 230006-250G
Nickel(II) nitrate hexahydrate	$Ni(NO_3)_2 \cdot 6H_2O$	99.999	203874-20G 203874-100G 203874-500G
Magnesium nitrate hexahydrate	$Mg(NO_3)_2 \cdot 6H_2O$	≥99.999	529362-25G
Copper(II) nitrate hydrate	$Cu(NO_3)_2 \cdot xH_2O$	99.999	229636-5G 229636-25G 229636-100G
Cupric nitrate hydrate	$Cu(NO_3)_2 \cdot 2.5 H_2O$	≥99.99	467855-50G 467855-250G
Cobalt(II) nitrate hexahydrate	$Co(NO_3)_2 \cdot 6H_2O$	99.999	203106-10G 203106-50G
Aluminum nitrate nonahydrate	$Al(NO_3)_3 \cdot 9H_2O$	99.997	229415-10G 229415-100G

Selected Solvents for Synthesis of Metal-Organic Frameworks

For a complete list of solvents offered by Sigma-Aldrich, please visit *sigma-aldrich.com*

Name	Structure	Purity (Assay) (%)	Cat. No.
N,N-Dimethylformamide		99.8	227056-100ML 227056-12X100ML 227056-1L 227056-6X1L 227056-2L 227056-4X2L 227056-18L 227056-200L
N,N-Dimethylformamide		≥99.8	437573-4X4L 437573-18L
N,N-Diethylformamide		99	186317-25G 186317-100G

Metal-Organic Frameworks (Basolite™)

For a complete list of materials for energy generation and storage, please visit *sigma-aldrich.com/renewable*

Name	BET Surf. Area (m²/g)	Particle Dimension (μm)	Cat. No.
Basolite A100	1100-1500	particle size distribution 31.55 (D50)	688738-10G 688738-100G 688738-500G
Basolite C 300	1500-2100	particle size distribution 15.96 (D50)	688614-10G 688614-100G 688614-500G
Basolite F300	1300-1600	-	690872-10G 690872-100G 690872-500G
Basolite Z1200	1300-1800	particle size 4.9 (D50)	691348-10G 691348-100G 691348-500G
Basosiv™ M050	400-600	-	713716-10G 713716-100G 713716-500G

For questions, product data, or new product suggestions, please contact Aldrich Materials Science at *matsci@sial.com*.

ALDRICH Chemistry

115

Sigma-Aldrich
3050 Spruce Street
St. Louis, MO 63103 USA
sigma-aldrich.com

Sigma-Aldrich Worldwide Offices

Argentina
Free Tel: 0810 888 7446
Tel: (+54) 11 4556 1472
Fax: (+54) 11 4552 1698

Australia
Free Tel: 1800 800 097
Free Fax: 1800 800 096
Tel: (+61) 2 9841 0555
Fax: (+61) 2 9841 0500

Austria
Tel: (+43) 1 605 81 10
Fax: (+43) 1 605 81 20

Belgium
Free Tel: 0800 14747
Free Fax: 0800 14745
Tel: (+32) 3 899 13 01
Fax: (+32) 3 899 13 11

Brazil
Free Tel: 0800 701 7425
Tel: (+55) 11 3732 3100
Fax: (+55) 11 5522 9895

Canada
Free Tel: 1800 565 1400
Free Fax: 1800 265 3858
Tel: (+1) 905 829 9500
Fax: (+1) 905 829 9292

Chile
Tel: (+56) 2 495 7395
Fax: (+56) 2 495 7396

China
Free Tel: 800 819 3336
Tel: (+86) 21 6141 5566
Fax: (+86) 21 6141 5567

Czech Republic
Tel: (+420) 246 003 200
Fax: (+420) 246 003 291

Denmark
Tel: (+45) 43 56 59 00
Fax: (+45) 43 56 59 05

Finland
Tel: (+358) 9 350 9250
Fax: (+358) 9 350 92555

France
Free Tel: 0800 211 408
Free Fax: 0800 031 052
Tel: (+33) 474 82 28 00
Fax: (+33) 474 95 68 08

Germany
Free Tel: 0800 51 55 000
Free Fax: 0800 64 90 000
Tel: (+49) 89 6513 0
Fax: (+49) 89 6513 1160

Hungary
Ingyenes telefonszám: 06 80 355 355
Ingyenes fax szám: 06 80 344 344
Tel: (+36) 1 235 9055
Fax: (+36) 1 269 6470

India
Telephone
Bangalore: (+91) 80 6621 9400
New Delhi: (+91) 11 4358 8000
Mumbai: (+91) 22 4087 2364
Hyderabad: (+91) 40 4015 5488
Kolkata: (+91) 33 4013 8000

Fax
Bangalore: (+91) 80 6621 9650
New Delhi: (+91) 11 4358 8001
Mumbai: (+91) 22 2579 7589
Hyderabad: (+91) 40 4015 5466
Kolkata: (+91) 33 4013 8016

Ireland
Free Tel: 1800 200 888
Free Fax: 1800 600 222
Tel: (+353) 402 20370
Fax: (+ 353) 402 20375

Israel
Free Tel: 1 800 70 2222
Tel: (+972) 8 948 4100
Fax: (+972) 8 948 4200

Italy
Numero Verde: 800 827018
Tel: (+39) 02 3341 7310
Fax: (+39) 02 3801 0737

Japan
Tel: (+81) 3 5796 7300
Fax: (+81) 3 5796 7315

Korea
Free Tel: (+82) 80 023 7111
Free Fax: (+82) 80 023 8111
Tel: (+82) 31 329 9000
Fax: (+82) 31 329 9090

Malaysia
Tel: (+60) 3 5635 3321
Fax: (+60) 3 5635 4116

Mexico
Free Tel: 01 800 007 5300
Free Fax: 01 800 712 9920
Tel: (+52) 722 276 1600
Fax: (+52) 722 276 1601

The Netherlands
Free Tel: 0800 022 9088
Free Fax: 0800 022 9089
Tel: (+31) 78 620 5411
Fax: (+31) 78 620 5421

New Zealand
Free Tel: 0800 936 666
Free Fax: 0800 937 777
Tel: (+61) 2 9841 0555
Fax: (+61) 2 9841 0500

Norway
Tel: (+47) 23 17 60 00
Fax: (+47) 23 17 60 10

Poland
Tel: (+48) 61 829 01 00
Fax: (+48) 61 829 01 20

Portugal
Free Tel: 800 202 180
Free Fax: 800 202 178
Tel: (+351) 21 924 2555
Fax: (+351) 21 924 2610

Russia
Tel: (+7) 495 621 5579
Fax: (+7) 495 621 5923

Singapore
Tel: (+65) 6779 1200
Fax: (+65) 6779 1822

Slovakia
Tel: (+421) 255 571 562
Fax: (+421) 255 571 564

South Africa
Free Tel: 0800 1100 75
Free Fax: 0800 1100 79
Tel: (+27) 11 979 1188
Fax: (+27) 11 979 1119

Spain
Free Tel: 900 101 376
Free Fax: 900 102 028
Tel: (+34) 91 661 99 77
Fax: (+34) 91 661 96 42

Sweden
Tel: (+46) 8 742 4200
Fax: (+46) 8 742 4243

Switzerland
Free Tel: 0800 80 00 80
Free Fax: 0800 80 00 81
Tel: (+41) 81 755 2828
Fax: (+41) 81 755 2815

United Kingdom
Free Tel: 0800 717 181
Free Fax: 0800 378 785
Tel: (+44) 1747 833 000
Fax: (+44) 1747 833 313

United States
Toll-Free: 800 325 3010
Toll-Free Fax: 800 325 5052
Tel: (+1) 314 771 5765
Fax: (+1) 314 771 5757

Vietnam
Tel: (+84) 3516 2810
Fax: (+84) 6258 4238

Internet
sigma-aldrich.com

Green Power

© Mixed Sources
Product group from well-managed forests, controlled sources and recycled wood or fiber
www.fsc.org Cert no. SGS-COC-003338
© 1996 Forest Stewardship Council
FSC
10%

Accelerating Customers'
Success through Innovation and
*Leadership in **Life Science,***
High Technology** and **Service

Order/Customer Service (800) 325-3010 • Fax (800) 325-5052
Technical Service (800) 325-5832 • *sigma-aldrich.com/techservice*
Development/Custom Manufacturing Inquiries SAFC® (800) 244-1173
Safety-related Information *sigma-aldrich.com/safetycenter*

World Headquarters
3050 Spruce St.
St. Louis, MO 63103
(314) 771-5765
sigma-aldrich.com

LZN
72680-508473
0119

SIGMA-ALDRICH®